Performance Evaluation of the Discrete Fourier Transform Based Beamformers Under Block and Sliding Window Processing Modes

Mehrab Khazraeiniay Allahdad

Submitted to the
Institute of Graduate Studies and Research
in partial fulfilment of the requirements for the degree of

Master of Science
in
Electrical and Electronic Engineering

Eastern Mediterranean University
September 2016
Gazimağusa, North Cyprus

Approval of the Institute of Graduate Studies and Research

Prof. Dr. Mustafa Tümer
Acting Director

I certify that this thesis satisfies all the requirements as a thesis for the degree of Master of Science in Electrical and Electronic Engineering.

Prof. Dr. Hasan Demirel
Chair, Department of Electrical and Electronic Engineering

We certify that we have read this thesis and that in our opinion it is fully adequate in scope and quality as a thesis for the degree of Master of Science in Electrical and Electronic Engineering.

Prof. Dr. Erhan A. İnce
Supervisor

Examining Committee

1. Prof. Dr. Hasan Amca

2. Prof. Dr. Erhan A. İnce

3. Prof. Dr. Osman Kükrer

ABSTRACT

The techniques that are used to make an array of sensors directive are known as beamforming techniques. Beamformers (BFs) have been designed to function as spatial-temporal filters. In this thesis, Capon's beamforming technique has been studied under both narrowband and broadband scenarios. To compensate for the propagation time of the signals to other antenna elements (under narrowband scenario) Minimum Variance BF (MVB) would apply a simple phase shift to each signal. This phase-shift corresponds to a correct time delay for one particular frequency only and can't be applied under the broadband scenario where multiple frequencies exist.

To achieve high spectral and spatial resolution over wideband channels a large number of sensors or tapped-delay-line elements would be required and this would inevitable cause an increase in computational complexity. Fortunately, this high computational complexity can be reduced by applying a transformation at TDL elements of each sensor. In this thesis we have used the Discrete Fourier Transform (DFT) to generate various frequency bins and have applied narrowband beamforming for each different bin. Frequency bins in the DFT-based broadband BF are created using Block Processing (BP) and Sliding Window processing (SW).

To evaluate the performance of the DFT-based BF, Ensemble Mean Squared Error (EMSE) and the Signal to Interference plus Noise Ratio (SINR) have been used. In addition, the thesis provides a comparison for the computational complexity of DFT-based BF under BP and SW modes. The complexity has been assessed in terms of the Multiply-ACcumulate (MAC) operations. For simulations MATLAB platform has

used. Three broadband incoming signals each with bandwidth $B = 50MHz$, central frequencies of $150\,MHz$ and DOAs of $\theta_1 = 20^{\circ}, \theta_2 = 40^{\circ}$ and $\theta_3 = -20^{\circ}$ were assumed. The signal with direction $\theta_1 = 20^{\circ}$ was marked as the desired signal and power of the three sources were respectively set to $P_{s_d} = 5,10,10(dBW/MHz)$. Each sensor's output was sampled at Nyquist rate of $1/2B$. For a fair comparison between the DFT based BF using BP and the DFT based BF using SW processing, the length of the signals were fixed to $N = 1000$ samples.

Simulation results show that the DFT-based BF under BP has higher proficiency in handling wideband signal sources. The SINRs at the output of the DFT-based BF was seen to be time varying (in fact periodic). On the other hand, the DFT-based BF utilizing SW processing would take one new snapshot under each iteration, and generate one sample at its output and would suffer from highly correlated inputs. DFT-based BF under SW processing would deliver lower SINRs in comparison to a DFT-based BF under BP when the window size and the block size are same.

Finally, the number of blocks or slides are the main factor in adjusting the computational complexities and accuracy of the estimated correlation matrices. Therefore, the size of blocks/slides should be selected carefully to meet certain criteria.

Keywords: Tapped Delay Line, DFT-based Beamformer, Block or Sliding Window Processing, SINR, Multiply-Accumulate Operations.

ÖZ

Dizilimli algılayıcıları belli bir yöne duyarlı kılmak için kullanılan tekniklere verilen ad hüzme oluşturma teknikleridir. Hüzme oluşturucular (BFs) birer uzamsal-zamansal süzgeç görevi yapmaları için tasarlanmışlardır. Bu tezde, en küçük değişintili hüzme oluşturucusu olarak da bilinen Capon hüzme oluşturma tekniği hem dar bant hem de geniş bant senaryoları altında çalışılmıştır. Dar bant senaryosu altında farklı sinyallerin anten elemanlarına yayılım zamanını denkleştirebimek için en küçük değişintili hüzme oluşturucusu (MV-BF) her sinyale basit bir faz kayması uygulamaktadır. Bu faz kayması her bir özel frekans için zamanda doğru bir gecikmeye denk geldiğinden çoklu frekansları barındıran geniş bant uygulamarında kullanılamamaktadır.

Geniş bant uygulamalarında yüksek spektrum çözünürlüğü veya uzamsal çözünürlük kazanabilmek için büyük sayıda algılayıcı veya dallı gecikme hattı elemanı gerekmekte, bu da kaçınılmaz olarak hesaplama karmaşıklığını artırmaktadır. İyidir ki, bu hesaplama karmaşıklığı her algılayıcıdaki dallı gecikme hattı elemanlarında bir dönüşüm uygulayarak azaltılabilmektedir. Bu tezde, farklı frekans seleleri yaratmak için her algılayıcıda ayrık Fourier dönüşümü uygulanmış ve her selede dar bantlı bir hüzme oluşturucu kullanılmıştır. Ayrık Fourier dönüşüm tabanlı hüzme oluşturucunun frekans seleleri bölük (BP) ve kayan çerçeve (SW) işleme biçimleri altında oluşturulmuştur.

Ayrık Fourier dönüşüm tabanlı hüzme oluşturucusunun başarımını değerlendirmk amaçlı ortalama karesel hatanın topluluk ortalaması (EMSE) ve sinyal-girişim artı gürültü-oranları (SINR) kullanılmıştır. Bunlara ek olarak, tezde ayrık Fourier dönüşüm

tabanlı hüzme oluşturucusunun BP ve SW modundaki hesaplama karmaşıklıkları kıyaslanmıştır. Karmaşıklık hesapları Çarpma-Biriktirme (MAC) işlemleri cinsinden gösterilmiştir. MATLAB platforumu üzerinde gerçekleştirilen benzetimlerde $\theta_1 = 20^{\circ}, \theta_2 = 40^{\circ}$ and $\theta_3 = -20^{\circ}$yönlerinden gelen ve bant genişlikleri ve merkez frekansları 50Mz ve 150 MHz olan üç farklı geniş bant sinyal varsayılmıştır (geliş yönü 20° olan sinyal istenen sinyaldir). Benzetimler esnasında kullanılan üç işaretin güçleri ise $P_{s_d} = 5, 10, 10(dBW/MHz)$ olarak alınmıştır. Alıcıda her algılayıcının çıktısı 1/2B olan Nyquist hızında örneklenmiştir. Benzetimlerde tüm işaret ve gürültü sinyalleri sıfır ortalamalı birbirinden ilintisiz beyaz Gauss süreçleri kullanarak gerçeklenmiştir. Ayrık Fourier dönüşüm tabanlı hüzme oluşturucusunun BP ve SW modlarında adil kıyaslanabilmesi için işaretlerin uzunlukları N = 1000 örnek olacak şekilde sabitlenmiştir.

Benzetim sonuçları BP modunda çalışan ayrık Fourier dönüşüm tabanlı hüzme oluşturucusunun geniş bantlı işaretleri işlerken daha başarılı olduğunu göstermiştir. Hüzme oluşturucusu çıktısındaki SINR değerlerinin zamanla değiştiği ve hatta periodik olduğu ve en iyi performansın her blokun ortasında elde edildiği gözlemlenmiştir. Ayrıca SINR değerlerinin blok başı ve sonunda en düşüktür. Diğer taraftan, SW modunda çalışan ayrık Fourier dönüşüm tabanlı hüzme oluşturucusu her döngüde sadece bir yeni enstantane aldığı ve çıktısında bir örnek yarattığı için yüksek ilintili girdiler sorun yaratmaktadır. Çerçeve genişliği ve bölük uzunluğu aynı olarak alınan durumlarda SW modundaki ayrık Fourier dönüşüm tabanlı hüzme oluşturucusunun BP modunda çalışana göre daha düşük SINRs değerleri verdiği görülmüştür.

Son olarak, hesaplama karmaşıklığı ve kestirilen ilinti matrislerinin doğruluğu bölük sayısına veya çerçeve sayısına endekslidir ve bu yüzden bölük ve çerçeve sayıları belli kriterleri yakalayabilmek için dikkatle seçilmelidir.

Anahtar Kelimeler: Dallı Gecikme Hattı, Ayrık Fourier Dönüşüm Tabanlı Hüzme Oluşturucu, Bölük veya Çerçeve İşleme Modu, SINR, Çarpma-Biriktirme İşlemleri.

DEDICATION

I would like to dedicate this thesis to family of mine. To my father, who taught me that the best kind of knowledge to have is that which is learned for its own sake. It is also dedicated to my mother, who taught me that even the largest task can be accomplished if it is done one step at a time. And I would like to dedicate this study to my sister, who is inspiring all over my life.

TABLE OF CONTENTS

LIST OF FIGURES

LIST OF TABLES

Chapter 1

INTRODUCTION

Processing the BeamFormers (BF) (spatial-temporal filters) carry out can be summarized in two steps: 1) synchronization 2) weight-and-sum [1]. The synchronization process is delaying or advancing each sensor output by an appropriate time such that the signal components coming from a desired direction are aligned (synchronized). Weight-and-sum process on the other hand assigns weights to each sensor output and sums them to get one yield. The synchronization is for controlling the steering direction and the weight-and-sum processing to control the beam-width of the main lobe.

As can be seen from Fig 1.1 BFs can be classified into four main groups. The first group looks at the bandwidth of the signal environment and classifies BFs as narrowband or broadband. The second group evaluates the closeness of the source and classifies BFs as near or far-field BFs [2]. The third group looks at the way the BF parameters have been selected and classifies the BFs as data independent and statistically optimum type [3]. For data independent beamforming only the direction of the desired signal is used as a-priori information while designing the beam. For statistically optimal BFs the coefficients are adjusted according to the array data while trying to optimize the array response according to some criteria such as the minimum mean squared error (MMSE). In general, the statistically optimum BFs place nulls in the directions of interfering sources in an attempt to maximize the Signal to

Interference plus Noise Ratio (SINR) at the BF output [3]. Better classification of statistically optimal BFs can also be achieved by considering the information used to modify BF coefficients. This information may include the direction of arrival (DOA) of a desired signal, the training sequence or the phase and amplitude collection of a transmitted data. An example for the statistically optimum BF is the Linearly Constrained Minimum Variance (LCMV) BF. The LCMV constrains the response of the BF to pass the signal from the intended direction with specific gain and phase. Contributions of interfering signals on the output is minimized by choosing a set of weights that minimizes the output power or the variance ($E\{|y|^2\} = \boldsymbol{w^H R_x w}$). LCMV formulation for choosing the weights can be written as:

$$\min_{\boldsymbol{w}} \ \boldsymbol{w^H} \mathbf{R}_x \boldsymbol{w} \ \ \text{s.t.} \ \ \boldsymbol{a^H}(\theta, \omega)\boldsymbol{w} = g^*, \tag{1.01}$$

where, $\boldsymbol{a}(\theta, \omega) = [1 \ \ e^{jw\tau_2\theta} \ \ e^{jw\tau_3\theta} \ \ \cdots \ \ e^{jw\tau_M\theta}]^H$ and g is a complex constant. The filter coefficients, ***w,*** can be obtained by solving (1.01) using the method of Lagrange multipliers and will be equal to:

$$\boldsymbol{w} = g^* \frac{\mathbf{R}_x^{-1}\boldsymbol{a}(\theta, \omega)}{\boldsymbol{a^H}(\theta, \omega)\mathbf{R}_x^{-1}\boldsymbol{a}(\theta, \omega)}. \tag{1.02}$$

Design of a beamforming system is important where received signals are mainly broadband and this impacts the speed of convergence, complexity, exactness and robustness of the BF. Figure 1.1 (d), classifies BFs based on how their coefficients are computed. Computations are carried out in time domain, in frequency domain and using sub-space methods [4], [5]. In general, implementation of a BF in time domain would lead to high computational complexity and slow convergence while computation of filter coefficients using either sub-spaces or the frequency domain would decrease this computational cost [6].

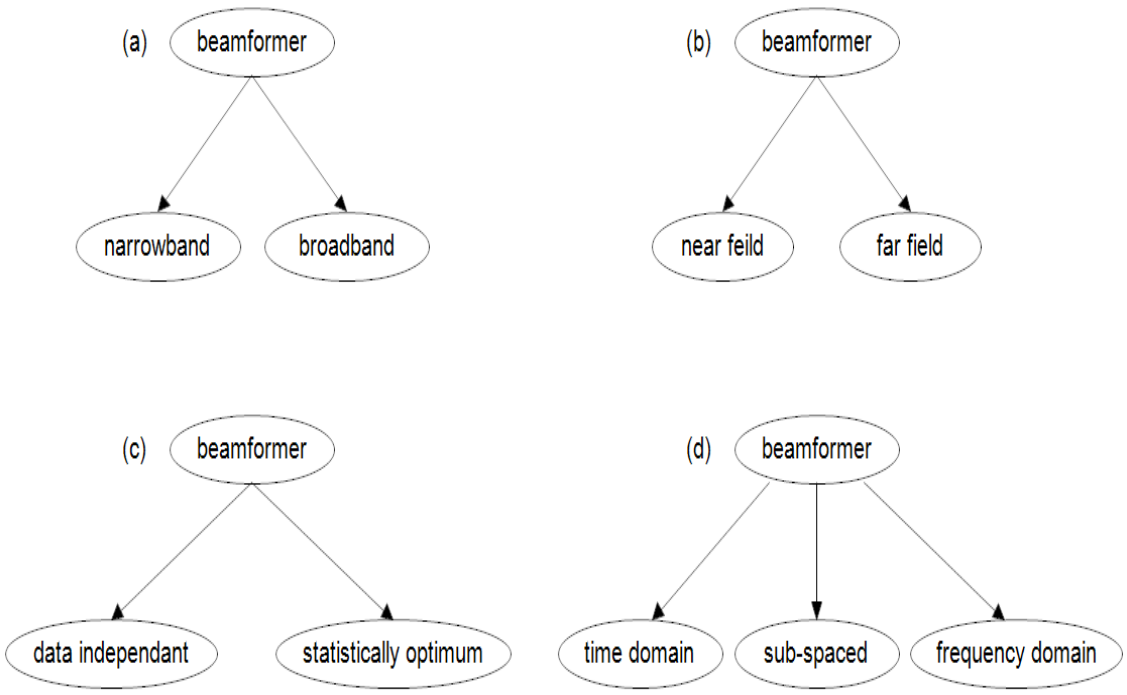

Figure 1.1: Various Ways of Classifying Beamformers.

In late decades, because of the increment in the bandwidth of emitted signals, evaluating the parameters of superimposed signals by using an arrangement of the sensors has turned into an interesting field of research and development in signal processing. Numerous theoretical reviews about broadband beamforming have been done, and profound information has been gathered as summarized by [7].

Beamformers which are directional arrays has the aim of focusing in a desired direction and they try to block out all interference and noise coming from other directions. However, in practice performance of adaptive antenna arrays can deteriorate due to: i) finite sample effect ii) correlated sources iii) steering vector faults etc. Many robust algorithms have been proposed to deal with these performance degrading effects. Most notable ones include spatial smoothing, signal blocking (or sliding), diagonal loading and eigenspace-based methods. Many methods are limited to the narrowband environment however applications such as sonar, radar and

communications are not necessarily narrowband. Because sources with non-zero bandwidths would degrade the performance of a sensor array, applying a broadband BF will become essential. BFs for reception of wideband signal can be categorized into two main structures: i) the Tapped Delay Line (TDL) structure and ii) the Discrete Fourier Transform (DFT) based BFs. In some publications the DFT-based BFs are referred to as the sensor-delay-line BFs.

Due to their efficiency, the TDL BFs have taken their place among some of the most popular BFs and are widely considered under broadband scenarios. With TDL structures time domain signals are strictly weighted by a set of coefficients which are obtained as a result of an optimization problem with certain constraints. Generally, a DFT-based BF transforms the received signals into the frequency domain by the concept of DFT and applies a narrowband BF to each frequency bin. In comparison to the TDL BF a DFT-based BF is computationally less complex since the dimensions of the matrices in has to invert is less when compared to the case of a TDL BF. In the literature, the performance of the DFT-based BF hasn't been considered in details. Furthermore, the performance of a DFT-based BF with estimated correlation matrices using finite number of samples has hardly been discussed or evaluated. Therefore, in this thesis we will examine the performance of a DFT-based BF under the wideband scenario when sample size is finite.

1.1 Thesis Outline

The contents of this thesis is organized as follows: Following a general introduction, the background survey and the description on how the thesis has been organized in Chapter1, Chapter 2 provides information on array signal processing, introduces the correlation based SINR measure and outlines the received signal model under

narrowband scenario. Chapter 3 introduces the Delay-And-Sum BeamFormer (DAS-BF) using TDL and Chapter 4 gives details about some beamforming methods for the narrowband case. The DFT-based broadband BF is studied in Chapter 5 and Chapter 6 provides simulation results under block processing (BP) and Sliding Window (SW) modes. Also, Chapter 5 explains the connection between the narrowband and broadband BFs in detail. Finally, Chapter 7 provides conclusions and makes suggestions for future work.

Chapter 2

ARRAY SIGNAL PROCESSING

A set of adjacent sensors (receivers) also known as an array of sensors are generally placed to follow a particular geometry and are used to observe and process electromagnetic or acoustic waves. As opposed to a single sensor scenario where the observation would be $(1 \times N)$ when an array with M sensors is used one would receive an observation of $(M \times N)$ and this increase in the size of observations would lead to enhanced estimations of parameters. For instance, in beamforming expanding the number of sensors to have more data in the same length signals would help to obtain better estimates for the correlation matrix and inherently to more accurate coefficient estimation for spatial filters. Consequently, SINR will be improved [8]. All computations and processing carried out using an array of sensors classify under array signal processing and tries to model a received signal by their temporal and spatial parameters. This information is then used to construct BFs [9]. Figure 2.1 (a) depicts a Uniform Linear Array (ULA) with element spacing of d units and without loss of generality, the first sensor is considered as the reference sensor. Figure 2.1 (b) shows a uniform circular array (UCA) with element spacing of $d = 2\pi D/\alpha$. Here D represents the number of elements in the array and α is the angle between the reference sensor and last element of the array [10].

2.1 Medium and Direction of Wave Field

Many natural phenomena result from the displacement of molecules. All of these

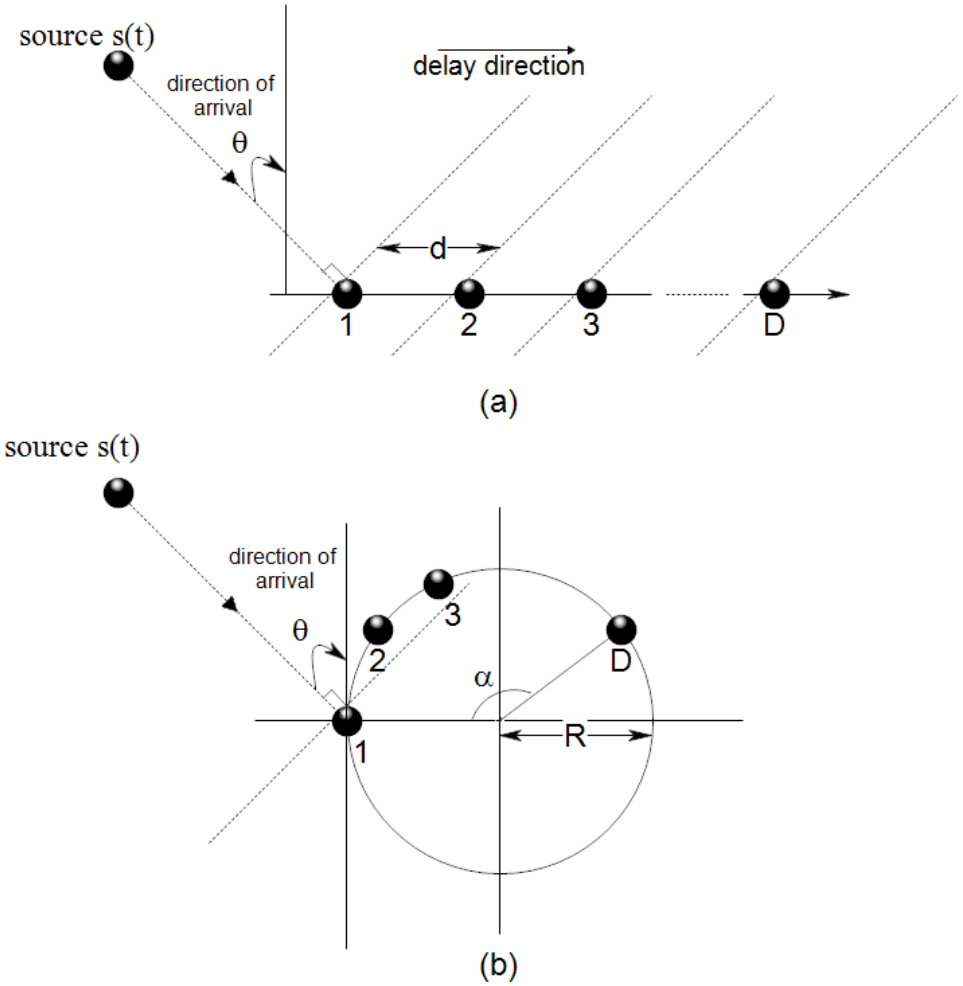

Figure 2.1: Linear and Circular Geometry Arrays that Have Uniform Spacing. (a) ULA with inter-element spacing of d, (b) UCA with received signal at direction θ to the reference sensor.

phenomena can be modeled by a wave field and formulated by wave propagation equations. Wave field propagation is a function of time and three-dimensional space which is expressed either in Cartesian or Spherical coordinates. While using Cartesian representation, signals are defined by three vectors along orthogonal axis $\boldsymbol{x}, \boldsymbol{y}$ and $\boldsymbol{z}$, on the other hand with spherical representation is defined by a scalar r which is equal to distance between a fixed origin and desired point in space, and two angles θ and $\emptyset$ where, θ represents the elevation angle $(0 \leq \theta \leq \pi)$ and $\emptyset$ is the azimuth angle $(0 \leq \emptyset \leq 2\pi)$. Transformations that map the spherical coordinates to

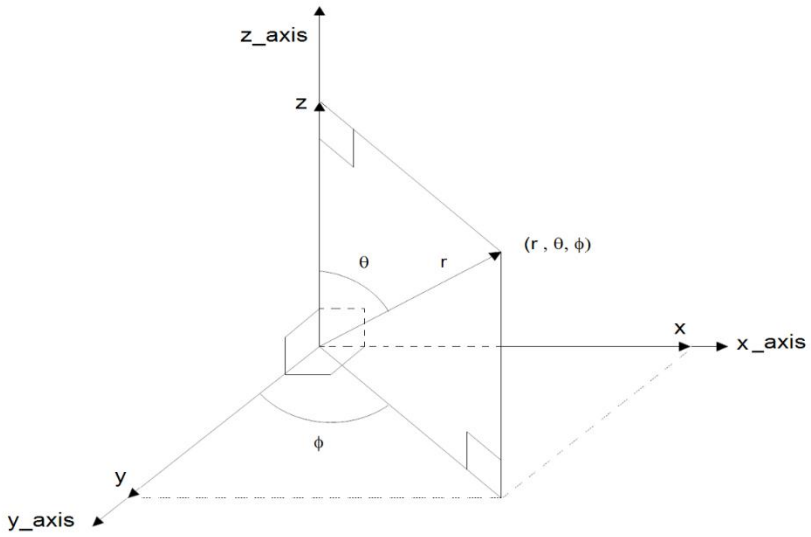

Figure 2.2: A 3-dimensional Representation with Cartesian Coordinates (x, y, z) and Spherical Coordinates (r, θ, Ø).

the Cartesian ones have been shown in (2.01) - (2.03) and visually depicted in Fig. 2.2.

$$\boldsymbol{x} = r \sin\theta \cos\emptyset\,, \tag{2.01}$$

$$\boldsymbol{y} = r \sin\theta \sin\emptyset\,, \tag{2.02}$$

$$\boldsymbol{z} = r \cos\theta \quad . \tag{2.03}$$

For any medium of propagation (2.04) describes propagated wave where $s(r,t)$ is emitted signal [11], (r,θ,ϕ) is the coordinate of the wavefront and t is the relevant time [12].

$$\nabla^2 s(r,t) = \frac{1}{c^2}\left(\frac{\partial^2 s(r,t)}{\partial t^2}\right), \tag{2.04}$$

the symbol c stands for the speed of propagated signal and ∇ denotes the Laplace operator. For an electromagnetic wave the propagation speed is approximately 3×10^8 ($^m/_s$). Given (2.04) we can solve for $s(r,t)$ and the emitted signal would have the form:

$$s(r,t) = A \exp[\mathrm{j}(\omega t - \boldsymbol{k}^T r)]. \tag{2.05}$$

Here A represents the amplitude of the emitted wave and is a constant, ω is the angular frequency and equals $2\pi f$ and $(.)^T$ denotes the transpose of a signal. Vector $\boldsymbol{k}$ is called wave-vector and is equal to $\boldsymbol{k} = \omega \cdot \boldsymbol{a}(\theta, \emptyset)$ where $\boldsymbol{a}(\theta, \emptyset)$ is called the slowness vector which describes the coordinates of the points in signal regarding to the azimuth and elevation angles [1]. It is easy to prove that $|\boldsymbol{k}| = \frac{\omega}{\pi} = \frac{2\pi}{\lambda}$ where λ is the wavelength, $2\pi/\lambda$ is the number of cycles per unit space (m) and $\boldsymbol{a}(\theta, \emptyset)$ represents direction of each cycle. Generally, when the observation points are nearby to the source the spherical representation would be used. In the case of a monochromatic spherical wave solution for (2.04) would be as in (2.06).

$$s(r,t) = \frac{A}{r} \exp\left[\mathrm{j}(\omega \mathrm{t} - |\boldsymbol{k}|r)\right]. \tag{2.06}$$

The homogeneity of the medium guarantees that the speed of propagation through the whole medium is remain constant. The dispersion-free medium guarantees that carrier frequency does not change from sender to receiver and lossless medium assumption assures that the medium will not modify the amplitude of the signals.

2.2 Emitted Signal

Assume that D signals originating from sources in different directions have been observed. One of these signals is the desired signal, and the remaining $(D-1)$ are interfering signals that are covered with white Gaussian noise. Based on [13], Hilbert transform of the received signal can be written as in (2.07):

$$x_I(t) = s_{1,I}(t+\tau_1) + s_{2,I}(t+\tau_2) + \ \dots\ \dots\ + s_{D,I}(t+\tau_D) + \boldsymbol{w}_I\,,$$

and (2.07)

$$x_Q(t) = s_{1,Q}(t+\tau_1) + s_{2,Q}(t+\tau_2) + \ \dots\dots + s_{D,Q}(t+\tau_D) + \boldsymbol{w}_Q\,.$$

In (2.07), $s_{d,I}(t)$ and $s_{d,Q}(t)$ where $1 \leq d \leq D$ are the in-phase and quadrature parts of the propagated signals, w_I and w_Q are in-phase and quadrature part of the corresponding noise, τ_d, $d \in [1,2,\cdots,D]$ are the duration times from D senders to the receiver. Throughout this thesis all sources will be assumed to be bandlimited and mutually uncorrelated and will be generated using white Gaussian distributions with zero mean and constant variance. Thus if all sources are bandlimited with central frequency f_c and bandwidth $2B$ then the in-phase quadrature parts of the emitted signals can written as:

$$s_{d,I}(t) = \alpha_d(t)\cos\big(2\pi f_c t + \varphi_d(t)\big),$$

$$s_{d,Q}(t) = \alpha_d(t)\sin\big(2\pi f_c t + \varphi_d(t)\big), \qquad 1 \leq d \leq D \quad (2.08)$$

where $\alpha_d(t)$ and $\varphi_d(t)$ represent the amplitude and carrier phase of the incoming signals.

2.3 Analytical Signal

In practice, sensors detect the in-phase part of the signal. Therefore by considering an array of sensors with M elements, analytical signal observed at the m^{th} element can be written as in (2.09):

$$\begin{aligned} x_{tot(m)}(t) &= x_{tot(I)}(t) + jx_{tot(\varphi)}(t) \\ &= \alpha_1\big(t + \tau_{1,m}\big)\exp\big\{2\pi f_c\big(t + \tau_{1,m}\big) + \varphi_1\big(t + \tau_{1,m}\big)\big\} + \\ &\quad \cdots \\ &\cdots + \alpha_D\big(t + \tau_{D,m}\big)\exp\big\{2\pi f_c\big(t + \tau_{D,m}\big) + \varphi_D\big(t + \tau_{D,m}\big)\big\} + \boldsymbol{w}_{tot(m)} \end{aligned}$$

$$m \in [1,2,\ldots,M], \quad (2.09)$$

where, $\tau_{d,m},\ d \in [1,2,\cdots,D]$ and $m \in [1,2,\cdots,M]$ is time taken by the signal to reach from d^{th} source to the m^{th} sensor of ULA and $\boldsymbol{w}_{tot(m)}$ is an additional noise to them^{th} sensor. After demodulating so that the signal is back in baseband, the output of the m^{th} sensor can be written as:

$$\begin{aligned} x_m(t) &= x_{tot(m)}(t)\exp\{-j2\pi f_c t\} \\ &= s_1\left(t+\tau_{1,m}\right)\exp\left\{j2\pi f_c \tau_{1,m}\right\} + \ \ldots \\ &\ldots + s_d\left(t+\tau_{D,m}\right)\exp\left\{j2\pi f_c \tau_{d,m}\right\} + \boldsymbol{w}_{tot(m)}\,. \end{aligned} \tag{2.10}$$

Furthermore, since the received signal is sampled at frequency $F_s = 1/T_s$ (2.10) could be re-written in its discrete representation as depicted by (2.11).

$$\begin{aligned} x_m(nT_s) &= x_{tot(m)}(nT_s)\exp\{j2\pi f_c t\} \\ &= s_1\left(nT_s+\tau_{1,m}\right)\exp\left\{j2\pi f_c \tau_{1,m}\right\} + \ \ldots \\ &\ldots + s_d\left(nT_s+\tau_{D,m}\right)\exp\left\{j2\pi f_c \tau_{d,m}\right\} + \boldsymbol{w}_{tot(m)}(nT_s). \end{aligned} \tag{2.11}$$

Throughout of this study, for convenience, variable nT_s from the sampled version of signals has replaced by an integer n. Without any confusion $x(nT_s) = x[n]$, where [.] denotes the discrete variable.

2.4 Finite Impulse Response

Various methods have been proposed in the literature to extract the desired signal (information) from a noisy sequence. In all methods the process of separating the desired signal from the received signal is referred to as filtering. Filters are generally characterized either by their impulse responses or frequency responses. For discrete-domain the number of tabs is fixed and hence the filter is referred to as a Finite Impulse Response (FIR) filter. The types of FIR filters are low-pass, high-pass, band-pass and bandstop. A low-pass filter permits frequencies beneath a predefined passband

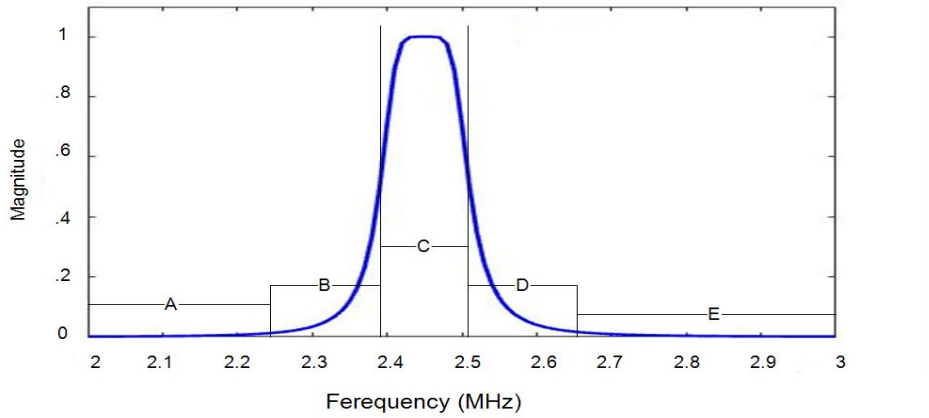

Figure 2.3: Band-pass Filter: (i) C Represents the Pass band, (ii) Section B and D Represent the Transition Bands and (iii) Parts A and E Denote the Stop bands.

frequency (ω_p) to pass and is used to kill the high frequencies. A high-pass filter does the inverse and attenuates the low frequencies and passes frequencies above ω_p. Bandpass and bandstop filters can be defined by a combination of low-pass and high-pass filters [14] and are used to either pass or stop a band of frequencies. Stopband filters are also known as notch filters.

2.5 Filters with Finite Impulse Response

The frequency response of an FIR filter is composed of three separate regions: namely (i) the pass band, (ii) the transition band and (iii) the stopband. Regions A-E in Fig 2.3 shows each one of these regions for a band-pass filter.

Considering an input sequence $\{x[n]\}$ as defined by (2.12) and a filter with M coefficients:

$$x[n] = \frac{A}{r} e^{j\emptyset} e^{j\omega n}\,, \tag{2.12}$$

the output $y[n]$ of the filter can be written as in (2.13)

$$y[n] = \sum_{k=0}^{M-1} b_k x(n-k)\,, \tag{2.13}$$

where, b_k represents the filter coefficients (tabs).

By inserting (2.12) into (2.13) frequency response of the FIR filter can be written in the form (2.17).

$$y[n] = \sum_{k=0}^{M-1} b_k \, A e^{j\emptyset} e^{j\omega(n-k)} \,, \tag{2.14}$$

$$y[n] = A e^{j\emptyset} e^{j\omega n} \sum_{k=0}^{M-1} b_k e^{-j\omega k} \,, \tag{2.15}$$

$$y[n] = x[n] H\left(e^{j\hat{\omega}_n}\right) \,, \tag{2.16}$$

$$H\left(e^{j\omega}\right) = \sum_{k=0}^{M-1} b_k e^{-j\omega k} \,. \tag{2.17}$$

2.6 Correlation-Based Signal to Interference Plus Noise Ratio

In the literature more often the Signal to Interference plus Noise Ratio (SINR) is used to evaluate the performance of a filter. SINR is based on the output power (P_x) of a signal $x[n]$. This output power can be calculated using (2.18):

$$P_x = E\{|\boldsymbol{x}|^2\} \,, \tag{2.18}$$

where $E\{\,.\,\}$ denotes the expected value function. Note that for convenience the time indexes have been dropped from equation (2.18). By inserting (2.16) into (2.18) the output power P_y for an FIR filter can be obtained as:

$$P_y = E\{|\boldsymbol{y}|^2\} \; = E\{\boldsymbol{y}\, \boldsymbol{y}^H\} = H\left(e^{j\omega}\right)^H E\{\boldsymbol{x}\, \boldsymbol{x}^H\}\, H\left(e^{j\omega}\right) . \tag{2.19}$$

Assuming a received signal that is Wide Sense Stationary (WSS), then the correlation function can be calculated using (2.20):

$$r_x = E\{\boldsymbol{x}\, \boldsymbol{x}^H\} \,. \tag{2.20}$$

If we denote the power spectral density of the time sequence $\boldsymbol{x}$ with $S(\omega)$, then in the $[-B, B]$ band r_x can be computed by taking the inverse Fourier transform of $S(\omega)$ as in (2.21) [15]:

$$r_x = \frac{1}{2\pi} \int_{-\infty}^{\infty} S(\omega) d\omega. \tag{2.21}$$

As (2.21) indicates the calculation of the correlation function requires an infinite number of samples. Since this is not practical actual correlation of a signal can't be obtained. Instead only an estimation of the correlation function is possible. How to estimate the correlation function given a fixed number of samples will be detailed in section 3.2.

2.7 Narrowband Definition

Without loss of generality if the bandwidth of a signal is much smaller than the central frequency, $i.e. B \ll f_c$, a signal can be considered as a narrowband signal [16] [17]. An alternative definition for narrowband signals has been provided by Zatman and is based on space decomposition for the covariance matrix.

Covariance matrix $\mathbf{R}_x$ can be decomposed to its eigenvalues and eigenvectors by the Singular Value Decomposition (SVD) algorithm as shown by (2.22):

$$\mathbf{R}_x = \mathbf{U}\, \Lambda\, \mathbf{U}^H . \tag{2.22}$$

Here, $\mathbf{U}$ represents a matrix that contains eigenvectors of the observed signal and Λ represents a diagonal matrix that contains eigenvalues $(\lambda_1, \lambda_2, \ldots, \lambda_N)$ of the received signal. These eigenvalues are ordered in descending format $(i.e. \lambda_1 \geq \lambda_2 \geq \ldots \geq \lambda_N)$. If one decomposes (2.22) into signal and noise sub-spaces, then (2.22) can be re-written as:

$$\mathbf{R}_x = \mathbf{U}_s \Lambda_s \mathbf{U}_s^H + \mathbf{U}_n \Lambda_n \mathbf{U}_n^H . \tag{2.23}$$

Here, the subscripts s and n respectively denote the signal and noise sub-spaces. Matrix $\mathbf{U}_s$ which contains the eigenvectors of the desired plus the interfering signals is known as the signal sub-space. For zero-bandwidth signal model (narrowband), the rank of signal sub-space is same as the number of the present signals. For broadband signals the viable rank of signal sub-space is larger than the number of signals [16].

For the narrowband case, the received signal model can be written as in (2.24)

$$x_m[n] = s_1[n]\exp\{j2\pi f_c\tau_{1,m}\} + \ \ldots\ldots + s_d[n]\exp\{j2\pi f_c\tau_{d,m}\} + \ \boldsymbol{w}_m[n]. \quad (2.24)$$

Thus, under narrowband scenario, the received signals to the m^{th} sensor can be modeled by a simple phase-shift $\{j2\pi f_c\tau_{d,m}\}$. In the following chapter we will show how $\tau_{d,m}$ is related to the distance between the d^{th} source and the m^{th} element of a sensor array.

Chapter 3

DELAY-AND-SUM BEAMFORMER

Delay-And-Sum Beamformer (DAS-BF) is a data independent BF in which the outputs from an array of sensors are time delayed so that when they are summed together, a particular portion of the received wave is amplified over other interfering sources. In what follows we introduce a model that shows the wavefront for a single source both in the near and far-fields and formulate the output for each sensor plus the filter in the far-field.

3.1 Signal Model for Uniform Linear Array

If we assume that there is a source s_1 in the far-field that is transmitting at an angle of θ as depicted by Fig 3.1 the wave front would be spherical near the source and as it travels further away from the source it will become a planar wave. For a ULA with M sensors, $x_m[n]$ for $1 \leq m \leq M$ represent the observation of the received signal by the m^{th} sensor. The sensor furthest to the left will capture the sound waves first. The adjacent sensors placed further to the right will receive the same signal, but with a slight time delay due to the additional distance sound waves must travel to get to the next sensors. If we denote the delay for each of the M sensors as $\{\tau_1(\theta), \tau_2(\theta), \cdots, \tau_{M-1}(\theta)\}$ then with the narrowband presumption (by setting zero delay between reference sensor and sources) (2.24) in Chapter-2 for the reference sensor can be re-written as: $x_{ref}[n] = s_1[n] + \cdots + s_D[n] + w_{ref}[n]$. Considering that the first sensor is the reference sensor then the delay between the m^{th} sensor of the array and the reference sensor could be calculated as:

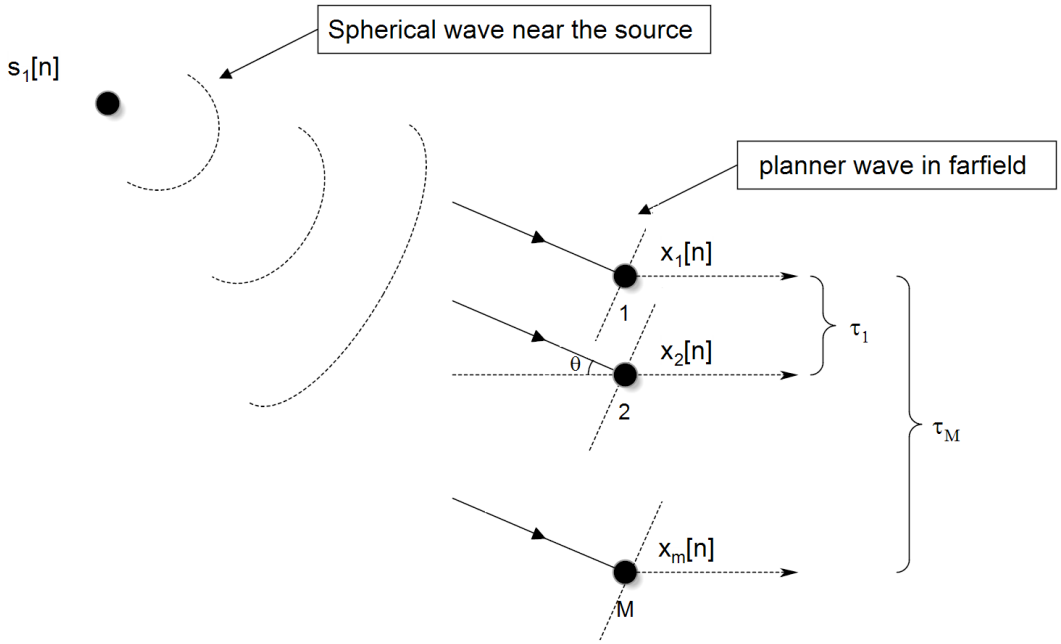

Figure 3.1: Signal Model for a Single Source Transmitting at Angle θ Towards a ULA Containing M Sensors.

$$\tau_m(\theta) = \frac{(m-1)d\ sin(\theta)}{c} \qquad 1 \le m \le M-1 \tag{3.01}$$

For the sake of simplicity in what follows we will drop the (θ) argument of the delays and simply write them as $\{\tau_1, \tau_2, \cdots, \tau_{M-1}\}$.

Furthermore, if we have D sources located at any direction, the observation by the m^{th} sensor of the ULA could be formulated as:

$$x_m[n] = s_1[n]\exp\{j2\pi f_c\tau_m\} + s_2[n]\exp\{j2\pi f_c\tau_m\} + \cdots + s_D[n]\exp\{j2\pi f_c\tau_m\} + w_m[n] \tag{3.02}$$

Similarly, for signals with *wide bandwidths* the observed sequence for a ULA with corresponding delays can be written as:

$$x_m[n] = s_1[n+\tau_m]\exp\{j2\pi f_c\tau_m\} + s_2[n+\tau_m]\exp\{j2\pi f_c\tau_m\} + \cdots + s_D[n+\tau_m]\exp\{j2\pi f_c\tau_m\} + w_m[n] \tag{3.03}$$

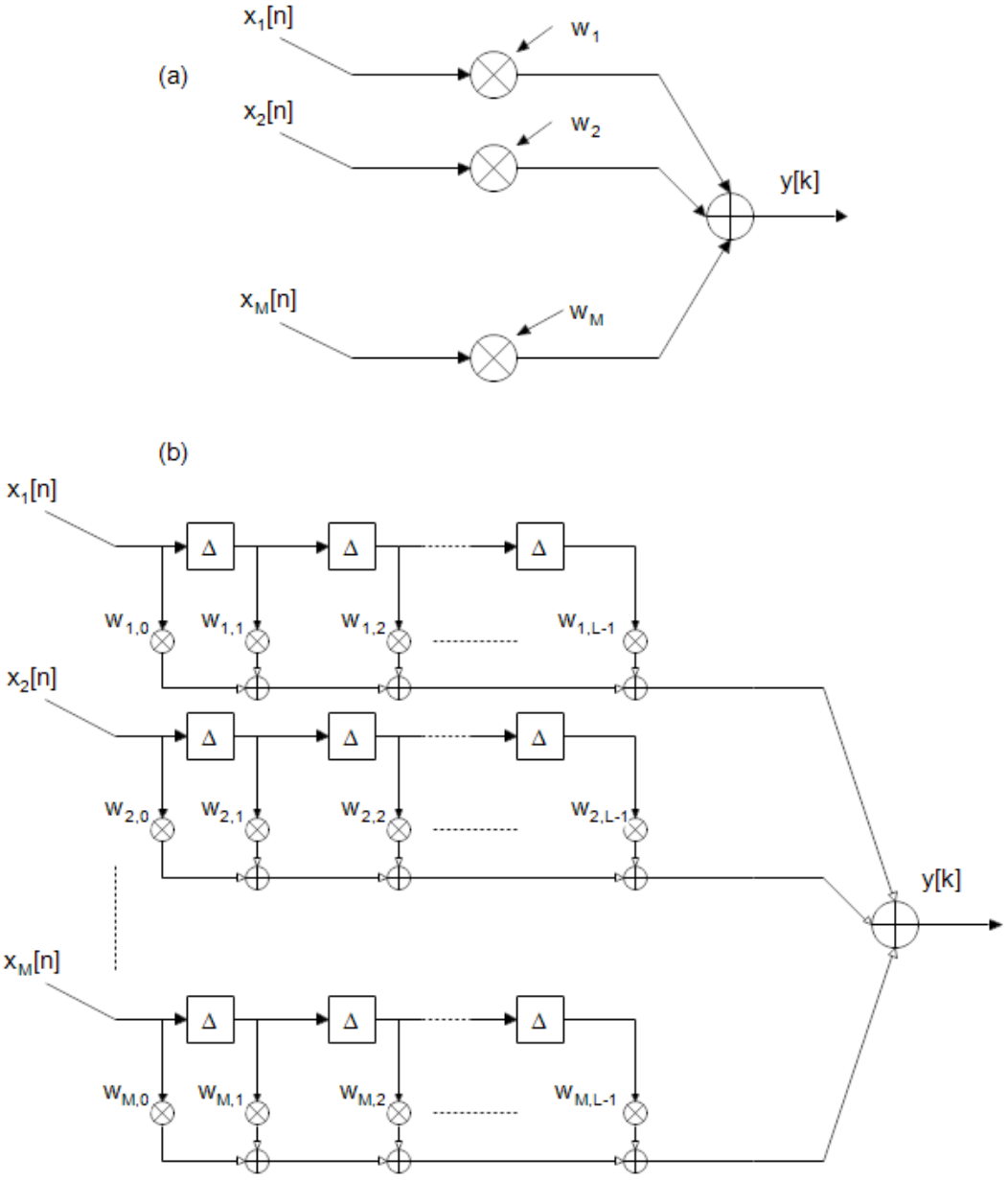

Figure 3.2: Delay-and-Sum Beamforming
(a) DAS beamformer under narrowband scenario,
(b) DAS beamformer under broadband scenario.

3.2 Delay-And-Sum Beamformer

Figure 3.2 (a) represents schematic for a DAS-BF under narrowband scenario, where $x_m[n]$ for $0 \leq n \leq N-1$ is the observed data by the m^{th} sensor. As depicted by the

$$y[n] = \sum_{m=1}^{M} \boldsymbol{w}_m^* \, x_m[n] \qquad 0 \leq n \leq N-1 \tag{3.04}$$

figure each observation will be multiplied by some weight factor that is related to the desired DOA. Afterwards the weighted observations are accumulated to form the output of the DAS-BF as in [8]. This is output has been formulated in (3.04).

The asterisk denotes the complex conjugate operator and w_m is the weight for the m^{th} sensor to adjust the output of the BF. We can say that (3.04) has M degrees of freedom (DOF) for steering M received signals. One of the DOFs is used to steer the desired signal and the others are used to suppress any interfering signals. Obviously, if the number of sources is greater than M then the system could only process M of these received signals and the rest are not processed.

If the signal passing through the adaptive weights has broadband characteristic, this structure proves ineffective since steering vector alone cannot provide a weighting such that all frequency components add up constructively as depicted by the narrowband BF in Fig. 3.2 (a) and an alternative structure is required. To resolve broadband signals, spatial-temporal flexibility must be enhanced and this is possible by applying a tapped-delay-line structure (finite impulse response filter) to the output of each sensor as depicted in Fig. 3.2 (b). Therefore under the broadband scenario the output y[n] of the BF can be written as:

$$y[n] = \sum_{m=1}^{M} \sum_{l=0}^{L-1} \boldsymbol{w}_{m,l}^{*}\, x_m[n-l]. \qquad 0 \le n \le N-1 \qquad (3.05)$$

Here the weights $w_{m,l}$ are used to filter each observation received by the m^{th} sensor of the ULA. The broadband BF has M DOF for steering M signals where each signal is passing through an L-tap FIR filter. This ability to sample the propagating wave both in space and time helps the BF resolve signals with broadband characteristics.

For convenience a common notation can be introduced for both narrowband and broadband beamforming structures of Fig. 3.2. The array outputs for (3.04) and (3.05) could be written as:

$$y[n] = \mathbf{W}^H \, \mathrm{x}[n] \tag{3.06}$$

$\mathbf{W}^H \in \mathrm{C}^{\mathrm{L}\times\mathrm{M}}$ holds all coefficients of the broadband BF (for all L TDLs). It is composed of M, size-L vectors where each vector $\boldsymbol{w}_m$ contains the complex conjugate coefficients of the FIR filter processing the signal observed at the m^{th} sensor of the ULA:

$$\mathbf{W}^H = \begin{bmatrix} w_1 \\ w_2 \\ \vdots \\ w_M \end{bmatrix} \tag{3.07}$$

$$\boldsymbol{w}_m = \left[w_{m,0}^*, w_{m,1}^*, \dots, w_{m,L-1}^*\right]^H \tag{3.08}$$

$\mathrm{x}[n]$, is a $(M \times L)$ matrix where the m^{th} row of $\mathrm{x}[n]$ represents the sample values in the tapped-delay-line for the m^{th} element of the ULA at discrete time *n*. Finally, $(\,.\,)^H$ represents the conjugate transpose operator. Hence $\mathrm{x}[n]$ can be written as:

$$\mathrm{x[n]} = \begin{bmatrix} x_1[0] & x_1[1] & \cdots & x_1[L-1] \\ x_2[0] & x_2[1] & \cdots & x_2[L-1] \\ \vdots & \vdots & & \vdots \\ x_M[0] & x_M[1] & \cdots & x_M[L-1] \end{bmatrix}. \tag{3.09}$$

By considering a DAS-BF as a spatial-temporal FIR filter with filter coefficients $\boldsymbol{w}_m$ for $1 \le m \le M$ and delays $\tau_m(\theta)$ as defined by (3.01), the frequency response of the DAS-BF can be expressed as:

$$H\left(e^{j\hat{\omega}}\right) = \sum_{m=1}^{M} \boldsymbol{w}_m^* e^{-j\hat{\omega}_c m}, \tag{3.10}$$

where $\hat{\omega}_c = \omega_c \cdot \tau_m(\theta)$. It is also possible to represent the frequency response of the DAS-BF in the form:

$$H\left(e^{j\hat{\omega}_c}\right) = \mathbf{W}^H \boldsymbol{a}\left(e^{j\hat{\omega}_c}\right), \tag{3.11}$$

where, $\boldsymbol{a}\left(e^{j\hat{\omega}_c}\right)$ is defined as:

$$\boldsymbol{a}\left(e^{j\hat{\omega}_c}\right) = \left[1 \quad e^{j\hat{\omega}_{c_1}} \quad \ldots \quad e^{j\hat{\omega}_{c_M}}\right]^H. \tag{3.12}$$

Finally, (3.12) can be written as:

$$\boldsymbol{a}\left(e^{j\hat{\omega}}\right) = \left[1 \;\; e^{j\tau_1(\theta)\omega_c} \;\; e^{j2\tau_1(\theta)\omega_c} \;\; \ldots \;\; e^{jM\tau_1(\theta)\omega_c}\right]^H. \tag{3.13}$$

In the literature $\boldsymbol{a}\left(e^{j\hat{\omega}_c}\right)$ is known as the steering vector or the manifold vector.

Since $\hat{\omega}_c$ is a function of time and wavelength the steering vector $\boldsymbol{a}\left(e^{j\hat{\omega}_c}\right)$ represents the spatial-temporal behavior of the FIR filter.

Assuming unit amplitude for a desired signal received from an angle of θ, the demodulated radio frequency (RF) signal observed by the m^{th} sensor of the antenna array can be represented as:

$$x_m[n] = e^{j\omega\left(n-\tau_m(\theta)\right)}. \quad 1 \le m \le M \tag{3.14}$$

Using (3.14) in (3.05) the output of the sensor array can be obtained as:

$$y[n] = \sum_{m=1}^{M} \sum_{l=0}^{L-1} \boldsymbol{w}_{m,l}^{*} \, e^{-j\omega\left(-n+l+\tau_m(\theta)\right)},$$

$$y[n] = e^{j\omega n} \sum_{l=0}^{L-1} \sum_{m=1}^{M} \boldsymbol{w}_{m,l}^{*} \, e^{-j\omega\tau_m(\theta)} e^{-j\omega l}, \tag{3.15}$$

$$y[n] = e^{j\omega n} \; H(\theta, \omega). \tag{3.16}$$

Therefore, the frequency response for the directional filter can be represented as:

$$H(\theta,\omega) = \sum_{l=0}^{L-1}\sum_{m=1}^{M} \boldsymbol{w}_{m,l}^{*}\, e^{-j\omega\tau_m(\theta)} e^{-j\omega l} \tag{3.17}$$

where,

$$H(\theta,\omega) = H\left(e^{j\hat{\omega}}\right)\sum_{l=0}^{L-1} e^{-j\hat{\omega}l} = H\left(e^{j\hat{\omega}}\right)\boldsymbol{a}(\theta,\omega)$$

Where,

$$\boldsymbol{a}(\theta,\omega) = \begin{bmatrix} 1 & e^{j\tau_1(\theta)\omega} & \dots & e^{j(L-1)\tau_m(\theta)\omega} \end{bmatrix}^{H} \tag{3.18}$$

Generally, the wave-vector $\boldsymbol{a}(\theta,\omega)$ is denoted as $\boldsymbol{a}(\theta)$.

Different sensors, ideal or not, can be made directional by using a steering vector. The steering vector describes the ULA's frequency response and the beam pattern is given by the square of the absolute value for $H(\theta,\omega)$.

Chapter 4

NARROWBAND BEAMFORMING

In the previous chapter we have showed how to obtain the steering vector for a BF both under narrowband and wideband scenarios. In this chapter we will describe the procedure for calculating the BF coefficients $(\boldsymbol{w}_k, 1 \leq k \leq M)$ under narrowband assumption. It is known that by weighting the signals from each sensor, it is possible to focus on signals arriving from a particular direction. However, the beamforming techniques differ in how they compute the weights and how they are applied. Weights can be computed either non-adaptively or using an adaptive process. Non-adaptive techniques are generally independent of the input data and can be considered as sub-optimal. Adaptive techniques on the other hand use the a-priori-statistics of the data and change, or adapt, in response to the data received before calculating the optimal weights.

In what follows we will focus on non-adaptive techniques and firstly introduce the conventional beamforming technique. Subsequent sections will summarize briefly the Minimum Variance Distortion-less Response (MVDR), the sub-space based MUltiple SIgnal Classification (MUSIC) algorithm and an extended version of the MUSIC algorithm. The chapter will also show how the weight vectors are obtained for each case.

4.1 Conventional Beamformer (CBf)

By assuming narrowband setting for the received signals, the usage of frequency diversity in received signal along the array is not critical, therefore (3.18) can be re-written based on the center frequency w_c as:

$$\boldsymbol{a}(\theta) = [1 \quad e^{j\omega_c\tau_1(\theta)} \quad \dots \quad e^{j\omega_c\tau_{m-1}(\theta)}]^H, \tag{4.01}$$

$\omega_c = 2\pi f_c$, and it is based the central-frequency f_c. For a transmitted signal matrix $S[n]$ which for D sources is represented as:

$$S[n] = \begin{bmatrix} S_1[n] \\ S_2[n] \\ \vdots \\ S_D[n] \end{bmatrix}. \tag{4.02}$$

The observation matrix can be defined as:

$$\mathrm{x[n]} = \boldsymbol{a}(\theta)S[\mathrm{n}] + N[\mathrm{n}]. \tag{4.03}$$

From (2.19) the output power of the BF will be:

$$P = \boldsymbol{w}^H \mathbf{R}_{\mathrm{x}} \boldsymbol{w}. \tag{4.04}$$

It is possible for the CBf to maximize its output power for a signal from a direction θ. Maximizing the output power in fact requires solving an optimization problem as depicted in (4.05)

$$\begin{aligned} \max_{w} [E\{\boldsymbol{w}^H \mathrm{x[n]x[n]}^H \boldsymbol{w}\}] &= \max_{w}[\boldsymbol{w}^H E\{\mathrm{x[n]x[n]}^H\}\boldsymbol{w}] \\ &= \max_{w}[E\{|S[\mathrm{n}]|^2 \times |w^H \boldsymbol{a}(\theta)|^2 + \sigma^2|\boldsymbol{w}|^2\}]. \end{aligned} \tag{4.05}$$

Here, σ^2 denotes the variance of the white noise assumed.

The output power of the CBf will be maximized when the weight vector is the same as the steering vector:

$$w_{CBf} = \boldsymbol{a}(\theta). \tag{4.06}$$

By placing (4.06) into (4.04) the output power of BF can be obtained as:

$$P_{CBf}(\theta) = \boldsymbol{a}^H(\theta)\mathbf{R}_x\,\boldsymbol{a}(\theta). \tag{4.07}$$

4.2 Minimum Variance Distortion-less Response Beamformer

In 1969, Capon came up with a new method now known as Capon's BF or MVDR BF. This new beamforming technique would define the filter coefficients by minimizing the output power of the ULA with respect to a unit gain constraint for a specific steering vector:

$$\begin{gathered} \min_{w}: P \\ s.t.\ \ \boldsymbol{w}^H\boldsymbol{a}(\theta) = 1\,. \end{gathered} \tag{4.08}$$

MVDR minimizes the power of received signals from undesired directions while the gain of the system at a desired direction is preserved. We can say that, MDVR select the coefficient from the space of the desired signal by setting the inner product of the coefficient basis and steering vector equal to one. This optimization problem can be solved using the method of Lagrange multipliers:

$$\int = \boldsymbol{w}^H \cdot \mathbf{R}_x \cdot \boldsymbol{w} + \lambda(\boldsymbol{w}^H \cdot \boldsymbol{a}(\theta) - 1),$$

$$\nabla_w \int = \nabla_w(\boldsymbol{w}^H\mathbf{R}_x\boldsymbol{w}) + \lambda \cdot \nabla_w\big(\boldsymbol{w}^H\boldsymbol{a}(\theta)\big) = 0,$$

$$\boldsymbol{w} = -\lambda \cdot \boldsymbol{a}(\theta)/\mathbf{R}_x\,,$$

$$\lambda = -\frac{1}{\boldsymbol{a}^H(\theta)\mathbf{R}_x^{-1}\,\boldsymbol{a}(\theta)}$$

Therefore, the optimal weight vector would be:

$$\mathbf{W}_{MDVR} = \frac{\mathbf{R}_x{}^{-1}\,\boldsymbol{a}(\theta)}{\boldsymbol{a}^H(\theta)\mathbf{R}_x{}^{-1}\,\boldsymbol{a}(\theta)}. \tag{4.9}$$

Consequently, the output power of the MVDR BF could be written as:

$$P_{MDVR}(\theta) = \frac{1}{\boldsymbol{a}^H(\theta)\,\mathbf{R}_x{}^{-1}\,\boldsymbol{a}(\theta)}. \tag{4.10}$$

We note that the CBf uses each and every opportunity to focus on the power of the desired signal in the look direction whereas the Capon's BF eliminates some noise which are perpendicular to the desired signal sub-space and puts a null in the orientation where there are interfering sources.

4.3 MUltiple SIgnal Classification (MUSIC) Beamformer

Even though various sub-space based beamforming techniques have been proposed one which has attracted tremendous attention was the Multiple Signal Classification (MUSIC) algorithm. This method makes use of the eigenstructure of the process and attempts to decompose the observation into two separate sub-spaces: namely signal sub-space and noise sub-space. Assuming WSS scenario and white noise the eigenvalue decomposition for the MUSIC algorithm can be stated as in [18]:

$$\mathbf{R}_x = \mathbf{U}_s \Lambda_s \mathbf{U}_s^H + \sigma^2 \mathbf{U}_n \mathbf{U}_n^H . \tag{4.11}$$

Matrix Λ_s include M largest eigenvalues of the observed signal and $\mathbf{U}_s$ the corresponding eigen-vectors. Similarly, U_n contains eigenvectors of the noise sub-space which are orthogonal to the signal sub-space. The orthogonality between signal and noise subspaces can be used to suppress the noise along the desired DOA by putting a null on the basis of noise subspace:

$$\mathbf{U}_n^H \boldsymbol{a}(\theta) = 0 . \tag{4.12}$$

On the other hand, the weight vector has to satisfy the non-singularity problem as follow:

$$\mathbf{W}^H \cdot \mathbf{W} = I. \tag{4.13}$$

For a ULA with M receiver, only M angel of arrivals can be steered by the BF therefore, the set $\{\theta_1 , \theta_2 , \dots \dots , \theta_M\}$ contains all possible solutions for (4.12). If they represent the orthogonal projection onto the noise subspace as:

$$\Pi^{\perp} = \mathbf{U}_n \mathbf{U}_n^H , \tag{4.14}$$

then, the output power of the BF using MUSIC algorithm for a specific direction can be calculated using:

$$P_{MUSIC}(\theta) = \frac{\boldsymbol{a}^H(\theta)\boldsymbol{a}(\theta)}{\boldsymbol{a}^H(\theta)\Pi^{\perp}\,\boldsymbol{a}(\theta)} . \tag{4.15}$$

For a ULA with M sensors, the steering vector(s) related to the M different DOAs ($\{\theta_1 , \theta_2 , \dots \dots , \theta_M\}$) would form a linearly independent set $\{a(\theta_1) , a(\theta_2), \dots , a(\theta_M)\}$. For unambiguity in the BF output, each DOA has to satisfy the inequality below and the distance between sensors has to be set as:

$$-\frac{\pi}{2} < \theta_m < \frac{\pi}{2} , m \in [1, M]; \quad \text{and} \quad d < \frac{\lambda}{2} . \tag{4.16}$$

For coherent and correlated signals the MUSIC algorithm which is designed to search for some orthogonal subspace to the noise subspace would give poor performance while it tries to extract the desired signal from the interfering signals.

4.4 Extentions to the MUltiple SIgnal Classification Beamformer

The extended research carried around the basic MUSIC algorithm has led to various adjustments. These adjustments were the outcomes of attempts to modify shortcomings of the original MUSIC algorithm under different scenarios. The most famous adjustment which led to the weighted MUSIC (W-MUSIC) algorithm was done to select a set of weights ($\mathbf{W}$) that could be used to consider the effect of different eigenvectors. The output power for the weighted music algorithm in terms of the steering vector and the selected weights is as:

$$P_{\mathrm{W-MUSIC}}(\theta) = \frac{\boldsymbol{a}^H(\theta)\boldsymbol{a}(\theta)}{\boldsymbol{a}^H(\theta)\widehat{\Pi}^{\perp}\,\mathbf{W}\,\widehat{\Pi}^{\perp}\,\boldsymbol{a}(\theta)}. \tag{4.17}$$

The novel weighting function **W** which is introduced to the spatial spectrum of the original MUSIC algorithm is a diagonal matrix where the diagonal elements are the characteristic vectors of the covariance matrix of the desired signal and $q \in [0,1]$:

$$\mathbf{W} = \begin{bmatrix} \lambda_1^q & 0 & \cdots & 0 \\ 0 & \lambda_2^q & 0 & \vdots \\ \vdots & 0 & \ddots & 0 \\ 0 & \cdots & 0 & \lambda_M^q \end{bmatrix}. \tag{4.18}$$

Range of q has been selected after extensive computer simulations and aims to reduce the covariance between the eigenvalues which then help the BF to better focus on a desired direction.

Gracefully, when the eigenvectors are uniformly weighted the W-MUSIC algorithm would converge to the standard MUSIC algorithm. The modified W-MUSIC algorithm provides an alternative to obtain better resolution for signals which are either highly correlated or under low SNR.

Chapter 5

DISCRETE FOURIER TRANSFORM BASED BROADBAND BEAMFORMER

Beamforming techniques have been thoroughly studied due to their usage in various application areas such as radar, sonar, biomedical and wireless communications. Since in practice the performance of the traditional DAS-BF is degraded due to high correlation between signals researchers have come up with the idea of spatial smoothing to improve the BF's performance. However, most of the studies have focused on beamforming under the narrowband scenario and the broadband issue hasn't been much studied. This chapter introduces a broadband BF which makes use of the discrete Fourier transform (DFT) concept to focus on a specific DOA for a given desired signal.

In any wave propagation medium (acoustic or electromagnetic) sensors can form a response pattern with higher sensitivity in a desired direction. An excellent data independent beam pattern is intended to reject interference signals and noise due to time sampling and position of sensors. One popular system for beam pattern configuration under broadband scenario is the frequency decomposition strategy. In this technique DFT is used to decompose the spectrum of a wideband signal into frequency containers or bins. What is in each bin is then taken into account as narrowband data.

5.1 Discrete Fourier Transform Based Beamformer

In the literature two variants of the DFT based BF has been proposed. These are namely: i) DFT-based BF using BP and ii) DFT-based BF using SW processing. The block diagram of the general DFT-based BF is depicted in Fig 5.1. As can be seen from the figure, at each sensor in the sensor array the received signal is first sampled using an analog to digital convertor and then the discrete signal is processed by a General Side-lobe Canceller (GSC) to produce uncorrelated sequences. Afterwards, the GSC's output is stored in a Length-*N* buffer and DFT of the samples in the buffer is taken. Following the DFT processing at each sensor, the DFT samples are weighed by BF weights at each sensor and $i^{th}, i \in [0, (N-1)]$ weighted samples of each sensor are accumulated to form the M inputs of the IDFT block.

For the case of D sources with arbitrary locations, the observed signal at the m^{th}element of the ULA given *N* snapshots of the received signal can be represented in a matrix form as:

$$\begin{aligned} \mathbf{x} &= [\ \ \mathbf{x}(0) \quad \mathbf{x}(1) \quad \ldots \quad \mathbf{x}(\mathrm{N}-1)\ ] \\ &= \begin{bmatrix} x_1(0) & x_1(1) & \cdots & x_1(N-1) \\ x_2(0) & x_2(1) & \cdots & x_2(N-1) \\ \vdots & \vdots & & \vdots \\ x_M(0) & x_M(1) & \cdots & x_M(N-1) \end{bmatrix} = \begin{bmatrix} \tilde{x}_1^T \\ \tilde{x}_2^T \\ \vdots \\ \tilde{x}_M^T \end{bmatrix}, \end{aligned} \tag{5.01}$$

where $(.)^{\mathrm{T}}$ denotes the transpose operation. After taking DFT along each row of the input matrix **x** the frequency domain matrix would be equal to:

$$\begin{aligned} \mathbf{X} &= [\ \ \mathrm{X}(0) \quad \mathrm{X}(1) \quad \ldots \quad \mathrm{X}(\mathrm{N}-1)\ ] \\ &= \begin{bmatrix} X_1(0) & X_1(1) & \cdots & X_1(N-1) \\ X_2(0) & X_2(1) & \cdots & X_2(N-1) \\ \vdots & \vdots & & \vdots \\ \vdots & \vdots & & \vdots \\ X_M(0) & X_M(1) & \cdots & X_M(N-1) \end{bmatrix}, \end{aligned} \tag{5.02}$$

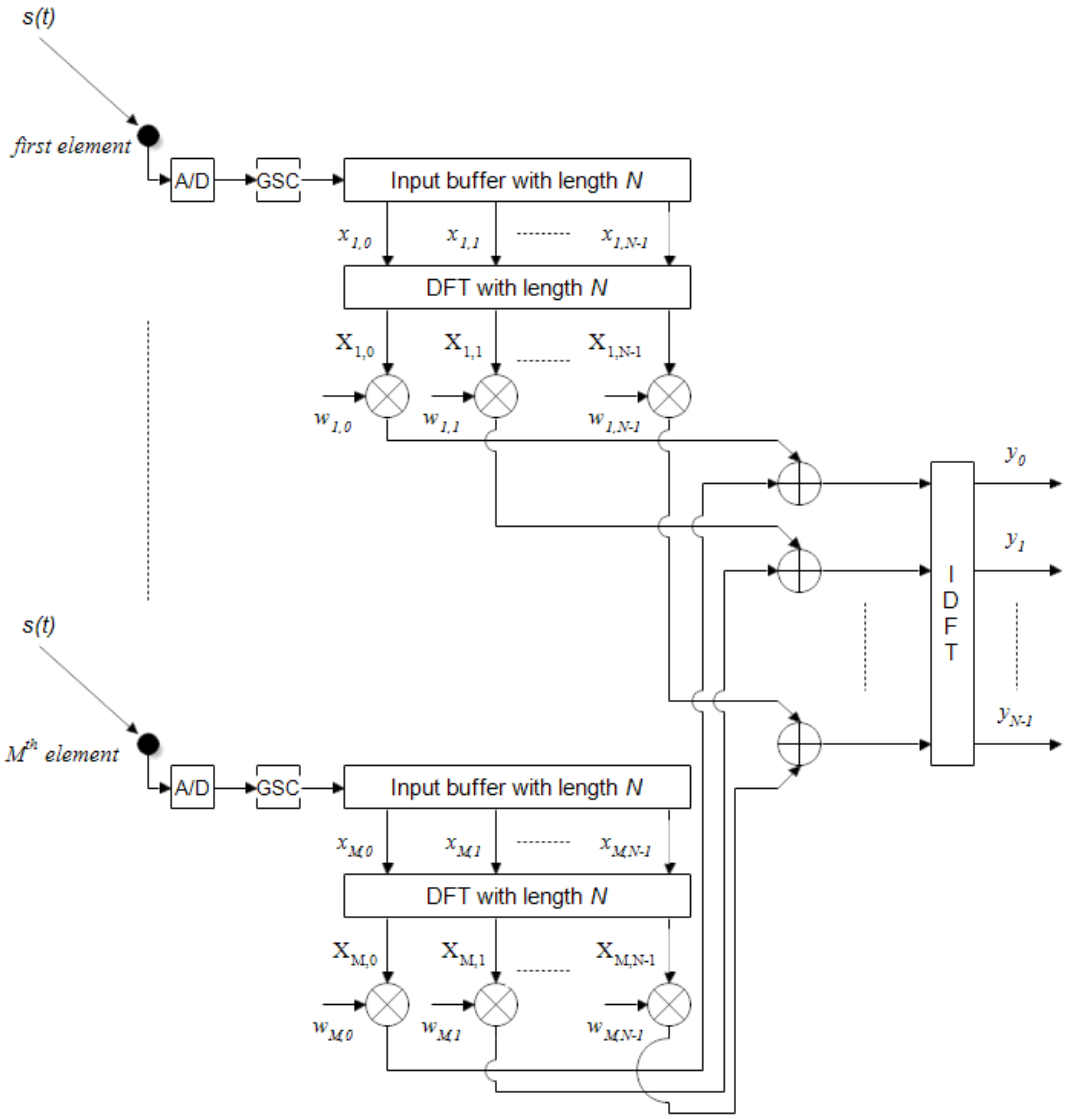

Figure 5.1: DFT-based Beamformer Using GSC with Buffer Length-N.

where $\mathrm{X}_m[k]$ is defined as:

$$\mathrm{X}_m[k] = \sum_{n=0}^{N-1} x_m[n]\, e^{-j2\pi nk/N} = e_k^H \tilde{x}_m \ , \qquad k = 0, 1, \ldots, (N-1). \tag{5.03}$$

Here m denotes the sensor in a sensor array with M sensors, index-n which ranges from 0 to $(N-1)$ denote the N samples and, k denotes the number of the frequency bin after the spectrum is divided into N narrower bands. The vector e_k for the k^{th} frequency bin can be expressed as:

$$e_k = \left[1 \;\; e^{j2\pi k/N} \ldots \;\; e^{j2\pi(N-1)k/N}\right]^T. \tag{5.04}$$

In (5.02) $\mathrm{X}[k] = \mathrm{X}[f_k]$ dedicates the $(k+1)$-th frequency bin of the observed data and for input signals with length-N, f_k can be expressed as:

$$f_k = \begin{cases} k.\Delta f & k = 0 : \left\lceil \frac{N}{2} \right\rceil - 1 \\ (k-N).\Delta f & k = \left\lceil \frac{N}{2} \right\rceil : (N-1) \end{cases}. \tag{5.05}$$

where the $\lceil . \rceil$ represents ceil operator and Δf denotes the frequency resolution and equals $\Delta f = \frac{1}{NT_s}$. Conceptually, Δf is the gap between frequency containers and better results is achievable by setting smaller gap between frequency bins. On the other hand, to avoid aliasing the sampling rate T_s is bounded by $2B$ where B denotes the bandwidth of the received signal. Hence for good resolution one must make sure that the number of samples (N) is large. By considering each frequency bin (f_k) as an individual data, it would be reasonable to apply a narrowband BF to each frequency bin. The output for each narrowband BF with weights $\mathbf{w}_k$ can then be formulated as:

$$\mathbf{Y} = \mathbf{w}_k^H \mathbf{X}[k],$$

$$\mathbf{Y} = [\,\mathrm{Y}(0)\;\; \mathrm{Y}(1)\;\; \mathrm{Y}(2)\;\; \ldots\;\; \mathrm{Y}(N-1)]. \tag{5.06}$$

Lastly, by taking the Inverse Discrete Fourier Transform (IDFT) of the weighted data **Y**, the output of the DFT-based BF in time domain can be written as:

$$\mathbf{y} = [\,y(0)\;\; y(1)\;\; y(2)\;\; \ldots\;\; y(N-1)],$$

$$y[n] = \frac{1}{N} \sum_{k=0}^{N-1} \mathrm{Y}[k] e^{j2\pi nk/N}, \qquad n = 0, \ldots, (N-1). \tag{5.07}$$

5.2 Generation of Steering Vector

If the signal bandwidth is small relative to the center frequency (i.e., if it has small fractional bandwidth), and the time intervals over which the signal is observed are short then we can use a narrowband BF to process the received signals. However, for

broadband signals temporal frequency analysis would be necessary at the BF. Hence the steering vector defined in (3.18) will take the form:

$$\mathrm{a}_k(\theta,\omega) = \left[1, e^{j2\pi(f_c+f_k)\tau_2(\theta)}, e^{j2\pi(f_c+f_k)\tau_3(\theta)}, \dots, e^{j2\pi(f_c+f_k)\tau_M(\theta)}\right]^H. \quad (5.08)$$

Consequently, by using the MVDR beamforming algorithm, the weight vectors for DFT based BF could be written as:

$$\boldsymbol{w}_k = \frac{\mathbf{R}_k^{-1}\boldsymbol{a}_k(\theta,\omega)}{\boldsymbol{a}_k^H(\theta,\omega)\mathbf{R}_k^{-1}\boldsymbol{a}_k(\theta,\omega)}, \quad (5.09)$$

here, $\mathbf{R}_k$ is the covariance matrix of the k^{th} bin and is as:

$$\mathbf{R}_k = E\{\mathbf{X}[k]\mathbf{X}^H[k]\}. \quad (5.10)$$

Since calculation of the covariance matrix ($\mathbf{R}_k$) in (5.10) would require unlimited snapshots (infinite number of samples) it can't be obtained via (5.10) and would be unknown. An approximate estimate of the covariance matrix $\mathbf{R}_k$ could still be obtained as stated in [19] using K-snapshots as:

$$\widehat{\mathbf{R}}_k = \frac{1}{N}\sum_{i=0}^{N-1} \mathbf{X}_{(i)}[k]\,\mathbf{X}_{(i)}{}^H[k]\,, \quad (5.11)$$

where, the subscript $(i), i = 0, 1, 2, \dots, (N-1)$ denotes the i^{th} snapshot of the k^{th} frequency component.

5.3 Block Processing for Discrete Fourier Transform Based Beamformer

For the DFT-based BF data across the sensor array at each frequency of interest must be processed separately by a narrowband sub-BF as depicted in Fig 5.2. In BP mode the algorithm needs to process J-blocks where each block has k_B snapshots. For a total of N-snapshots coming from the sensor array, the number of snapshots per block

would be equal to $\left\lfloor \frac{N}{J} \right\rfloor$ where $\lfloor \cdot \rfloor$ represents the flooring operation. Thus 5.01 can be written as:

$$\mathbf{x}_{\boldsymbol{AB}} = \begin{bmatrix} x_1(0) & x_1(1) & \dots & x_1(k_B-1) & x_1(k_B) & \dots & x_1(2k_B-1) & \dots & x_1(Jk_B-1) \\ x_2(0) & x_2(1) & \dots & x_2(k_B-1) & x_2(k_B) & \dots & x_2(2k_B-1) & \dots & x_2(Jk_B-1) \\ \vdots & \vdots & \vdots & \vdots & \vdots & \vdots & \vdots & \vdots & \vdots \\ x_M(0) & x_M(1) & \dots & x_M(k_B-1) & x_M(k_B) & \dots & x_M(2k_B-1) & \dots & x_M(Jk_B-1) \end{bmatrix}. \quad (5.12)$$

The subscript $\boldsymbol{AB}$ denotes the J-blocks in the BP mode.

Note that in BP mode each block $\mathbf{X}_{(j)}$ can be denoted as:

$$\mathbf{x}_{(j)} = \begin{bmatrix} x_1\big((j-1)k_B\big) & x_1\big((j-1)k_B+1\big) & \dots & x_1(jk_B-1) \\ x_2\big((j-1)k_B\big) & x_2\big((j-1)k_B+1\big) & \dots & x_2(jk_B-1) \\ \vdots & \vdots & \vdots & \vdots \\ x_M\big((j-1)k_B\big) & x_M\big((j-1)k_B+1\big) & \dots & x_M(jk_B-1) \end{bmatrix}. \quad (5.13)$$

And the full set of data is:

$$\mathbf{x}_{AB} = \begin{bmatrix} \mathbf{x}_{(1)} & \mathbf{x}_{(2)} & \dots & \mathbf{x}_{(J)} \end{bmatrix}.$$

It is evident that the length of observation has to be an integer product of the block size. Consequently, the DTF of the observed signal under BP mode could be expressed as:

$$\mathbf{X}_{AB} = \begin{bmatrix} \mathbf{X}_{(1)} & \mathbf{X}_{(2)} & \dots & \mathbf{X}_{(J)} \end{bmatrix}, \quad (5.14)$$

where, $$\mathbf{X}_{(j)} = \begin{bmatrix} X_1\big((j-1)k_B\big) & X_1\big((j-1)k_B+1\big) & \dots & X_1(jk_B-1) \\ X_2\big((j-1)k_B\big) & X_2\big((j-1)k_B+1\big) & \dots & X_2(jk_B-1) \\ \vdots & \vdots & \vdots & \vdots \\ X_M\big((j-1)k_B\big) & X_M\big((j-1)k_B+1\big) & \dots & X_M(jk_B-1) \end{bmatrix}.$$

The covariance matrix estimation for the DFT based BF under BP mode can be defined as:

$$\widehat{\mathbf{R}}_k = \frac{1}{J} \sum_{i=1}^{J} \mathbf{X}_{(i)}[k]\, \mathbf{X}_{(i)}^{H}[k], \qquad k = 0, 1, 2, \dots, (k_B - 1). \quad (5.15)$$

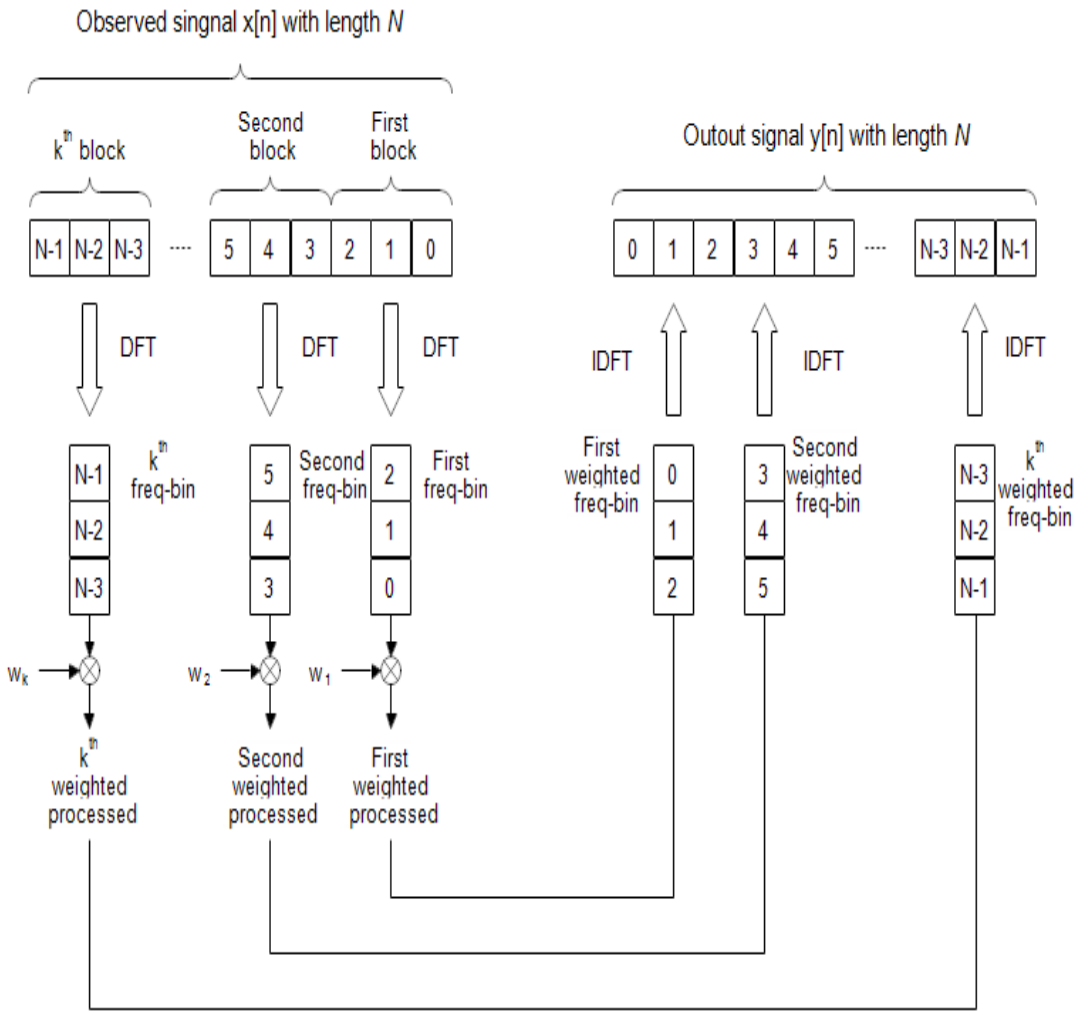

Figure 5.2: DFT-based Beamformer Using Block Processing Mode

Moreover, by inserting (5.15) in (5.09), the weight vectors for BP could be denoted as:

$$\boldsymbol{w}_k = \frac{\widehat{\mathbf{R}}_k^{-1}\boldsymbol{a}_k(\theta,\omega)}{\boldsymbol{a}_k^H(\theta,\omega)\widehat{\mathbf{R}}_k^{-1}\boldsymbol{a}_k(\theta,\omega)}, \qquad k = 0, 1, 2, \dots, (k_B - 1). \tag{5.16}$$

Finally, IDFT will be used to obtain the BF output in time-domain for each block. The output in BP mode is as follows:

$$y_{(j)}[n] = \frac{1}{k_B}\sum_{k=0}^{k_B-1} \boldsymbol{w}_k^H\, \mathbf{X}_{(j)}[k]\, e^{j2\pi nk/k_B}, \tag{5.17}$$

$$n = 0, \dots, (k_B - 1), \quad j = 1, \dots, J.$$

5.4 Sliding Window Mode for Discrete Fourier Transform Based Beamformer

For the DFT based BF the SW processing is similar to that of the BP mode. These two modes differ in the way they estimate the covariance matrix. In SW processing when a new snapshot arrive the oldest snapshot will be pulled out and the new one inserted into the data set. Afterwards the same processing in BP mode will be carried out. However, during batch processing no new snapshots would in reality arrive. To account for accepting the new snapshot and discarding the oldest one the algorithm will reserve the first $(N-J)$ snapshots into the first window and afterwards slide the window to the right by one snapshot at each step. Figure 5.3 illustrates the sliding procedure for $\mathbf{x}[n]$ defined in (5.18):

$$\mathrm{x} = \begin{bmatrix} x_1(0) & x_1(1) & \dots & x_1(k_S+J-1) \\ x_2(0) & x_2(1) & \dots & x_2(k_s+J-1) \\ \vdots & \vdots & \vdots & \vdots \\ x_M(0) & x_M(1) & \dots & x_M(k_S+J-1) \end{bmatrix}, \tag{5.18}$$

$$\mathbf{x}_{(j)_{SM}} = \begin{bmatrix} x_1(j-1) & x_1(j) & \dots & x_1(k_S+j-2) \\ x_2(j-1) & x_2(j) & \dots & x_2(k_S+j-2) \\ \vdots & \vdots & \vdots & \vdots \\ x_M(j-1) & x_M(j) & \dots & x_M(k_S+j-2) \end{bmatrix},$$

$$k_S = (N-J), \qquad 1 \le j \le J.$$

After taking DFT of each slide the spectrum of slides will be denoted as:

$$\mathbf{X}_{(j)} = \begin{bmatrix} X_1(j-1) & X_1(j) & \dots & X_1(k_S+j-2) \\ X_2(j-1) & X_2(j) & \dots & X_2(k_S+j-2) \\ \vdots & \vdots & \vdots & \vdots \\ X_M(j-1) & X_M(j) & \dots & X_M(k_S+j-2) \end{bmatrix}, \ 1 \le j \le J. \tag{5.19}$$

An estimate of the covariance matrix under SW processing can then be defined as:

$$\widehat{\mathbf{R}}_k = \frac{1}{J} \sum_{i=1}^{J} \mathbf{X}_{(i)}[k]\, \mathbf{X}_{(i)}^{H}[k], \qquad k = 0, 1, 2, \dots, (k_s - 1). \tag{5.20}$$

By inserting (5.20) in (5.09) the weight vectors under SW processing could be

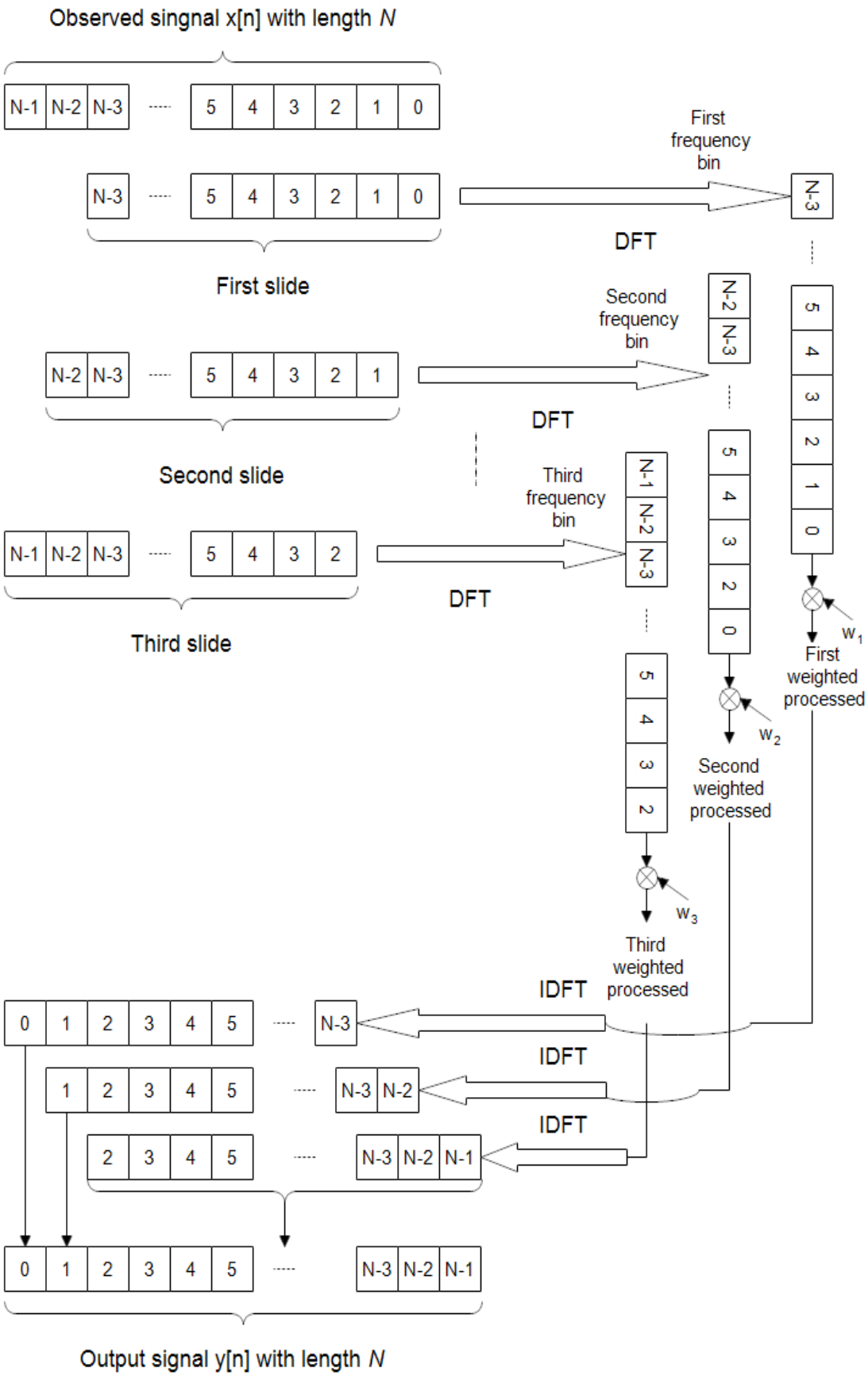

Figure 5.3: DFT-based Beamformer Under Sliding Window Processing

written as:

$$\boldsymbol{w}_k = \frac{\widehat{\mathbf{R}}_k^{-1}\boldsymbol{a}_k(\theta,\omega)}{\boldsymbol{a}_k^H(\theta,\omega)\widehat{\mathbf{R}}_k^{-1}\boldsymbol{a}_k(\theta,\omega)}, \qquad k = 0,1,2,\dots,(k_s-1). \tag{5.21}$$

Consequently, the output of the DFT-based BF under SW processing for each slide becomes:

$$y_{(j)}[n] = \frac{1}{k_S}\sum_{k=0}^{k_S-1} \boldsymbol{w}_k^H\, \mathbf{X}_{(j)}[k]\, e^{j2\pi nk/k_S},$$

$$n = 0,\dots,(k_s-1),\ \ j = 1,\dots,J. \tag{5.22}$$

5.5 Signal to Interference Plus Noise Ratio Formulation for the DFT-Based Beamformer Under Block Processing

Under DFT-based beamforming applying IDFT to each block of the output received from an M-element sensor array will result in a length-N output in the time-domain. The final output of the DFT-based BF can be expressed as in (5.23):

$$y_{(j)}[n] = \frac{1}{k_B}\sum_{k=1}^{k_B-1} \boldsymbol{w}_k^H\, \mathbf{X}_{(j)}[k]\, e^{j2\pi nk/k_B},$$

$$n = 0,\dots,(k_B-1),\quad j = 1,\dots,J,$$

$$\boldsymbol{y} = \left[y_{(1)}\ y_{(2)}\ \cdots\ y_{(J)}\right],$$

$$\boldsymbol{y} = \frac{1}{N}\,\boldsymbol{w}^H\, F_n\, \mathbf{X}_{|}, \tag{5.23}$$

where $\boldsymbol{w}^H$ and $\mathbf{X}_{|}$ are column vectors each with size $\left((M\cdot k_B)\times 1\right)$ as shown below:

$$\boldsymbol{w} \triangleq \left[w_0^T\ \ w_1^T\ \ \dots\ \ w_{k_B-1}^T\right]^T. \tag{5.24}$$

$$\mathbf{X}_{|} \triangleq \left[\mathrm{X}^T[0]\ \ \mathrm{X}^T[1]\ \ \dots\ \ \mathrm{X}^T[k_B-1]\right]^T, \tag{5.25}$$

The operator matrix F_n, $1 \le n \le J$ shown in (5.23), can be considered as an IDFT operation for each block with fixed dimension $(M \cdot k_B \times M \cdot k_B)$, and can be expressed as:

$$F_n \triangleq \begin{bmatrix} \boldsymbol{I}_M & 0 & & \dots & 0 \\ 0 & e^{j2\pi n/k_B}.\boldsymbol{I}_M & & & \vdots \\ \vdots & & \ddots & & 0 \\ 0 & \dots & 0 & e^{j2\pi(k_B-1)/k_B}.\boldsymbol{I}_M & \end{bmatrix} = diag(e_n) \otimes \boldsymbol{I}_M \,, \qquad (5.26)$$

where $\boldsymbol{I}_M$ denotes an $(M \times M)$ identity matrix and $\otimes$ denotes the Kronecker product. The vector e_n for $0 \le n \le (k_B - 1)$ has form:

$$e_n = \begin{bmatrix} 1 & e^{j2\pi n/k_B} & e^{j2\pi 2n/k_B} & e^{j2\pi 3n/k_B} \dots & e^{j2\pi(k_B-1)n/k_B} \end{bmatrix}^T. \qquad (5.27)$$

Obviously, e_n is a column vector with size $(k_B \times 1)$, hence $diag(e_0)$ would be:

$$diag(e_0) = \begin{bmatrix} 1 & 0 & & 0 \\ \vdots & \vdots & \cdots & \\ 1 & 0 & & \vdots \\ 0 & 1 & & \\ \vdots & \vdots & & \\ & 1 & & \\ & & \ddots & 0 \\ \vdots & 0 & & 1 \\ & & & \vdots \\ 0 & \cdots & & 1 \end{bmatrix}.$$

By substituting (5.23) into (2.19), the output power of the signal can be calculated as:

$$P = E\{|\boldsymbol{y}|^2\} = \frac{1}{(k_B)^2}\, \boldsymbol{w}^H F_n E\left\{\mathbf{X}_{|}\mathbf{X}_{|}^H\right\} F_n^H \boldsymbol{w} \,, \qquad (5.28)$$

where,

$$E\left\{\mathbf{X}_{|}\mathbf{X}_{|}^H\right\} \triangleq \mathbf{R}_{|} \,. \qquad (5.29)$$

Since expected value function is a linear function the covariance matrix $\boldsymbol{R}_{|}$ can be re-stated as:

$$\mathbf{R}_{|} = \begin{bmatrix} E\{X[0]X^H[0]\} & E\{X[0]X^H[1]\} & \dots & E\{X[0]X^H[k_B-1]\} \\ E\{X[1]X^H[0]\} & E\{X[1]X^H[1]\} & \dots & E\{X[1]X^H[k_B-1]\} \\ \vdots & \vdots & & \vdots \\ E\{X[k_B-1]X^H[0]\} & E\{X[k_B-1]X^H[1]\} & \dots & E\{X[k_B-1]X^H[k_B-1]\} \end{bmatrix}. \quad (5.30)$$

The covariance matrix $\mathbf{R}_{|}$ contains N^2 sub-matrices each with $(M \times M)$ dimension and represents the covariance between frequency bins i and j, $i = 0, \dots, (k_B - 1)$ and $j = 0, \dots, (k_B - 1)$. Hence, the overall covariance matrix between all frequency bin pairs can be denoted as follow:

$$E\{X[i]X^H[j]\} = \begin{bmatrix} E\{X_1[i]X_1^*[j]\} & E\{X_1[i]X_2^*[j]\} & \dots & E\{X_1[i]X_M^*[j]\} \\ E\{X_2[i]X_1^*[j]\} & E\{X_2[i]X_2^*[j]\} & \dots & E\{X_2[i]X_M^*[j]\} \\ \vdots & \vdots & & \vdots \\ E\{X_M[i]X_1^*[j]\} & E\{X_M[i]X_2^*[j]\} & \dots & E\{X_M[j]X_M^*[j]\} \end{bmatrix},$$

$$i = 0, \dots, (k_B - 1), \qquad j = 0, \dots, (k_B - 1) \quad (5.31)$$

where $(\,.\,)^*$ denotes the conjugate transpose operator. The matrix in (5.31) is composed of M^2 sub-matrices such as $E\{X_m[i]X_n^*[j]\}$ where,

$$E\{X_m[i]X_n^*[j]\} = e_i^H E\{\tilde{x}_m \tilde{x}_n^H\} e_j,$$

$$i = 0, \dots, (k_B - 1), j = 0, \dots, (k_B - 1), m = 1, \dots, M \text{ and } n = 1, \dots, M. \quad (5.32)$$

Denoting the expected value of signals received from sensors m and n as: $\mathrm{E}\{\tilde{\mathrm{x}}_m \tilde{\mathrm{x}}_{\mathrm{n}}^H\} = \mathrm{R}_{m,\mathrm{n}}$, $(m = 1, \dots, M \text{ and } n = 1, \dots, M)$ and substituting (5.31) into (5.30) the covariance matrix between frequency bins i and j, $i = 0, \dots, (k_B - 1)$ and $j = 0, \dots, (k_B - 1)$ could be expressed as:

$$E\{X[i]X^H[j]\} = \begin{bmatrix} e_i^H \mathbf{R}_{1,1} e_j & e_i^H \mathbf{R}_{1,2} e_j & \dots & e_i^H \mathbf{R}_{1,M} e_j \\ e_i^H \mathbf{R}_{2,1} e_j & e_i^H \mathbf{R}_{2,2} e_j & \dots & e_i^H \mathbf{R}_{2,M} e_j \\ \vdots & \vdots & \ddots & \vdots \\ e_i^H \mathbf{R}_{M,1} e_j & e_i^H \mathbf{R}_{M,2} e_j & \dots & e_i^H \mathbf{R}_{M,M} e_j \end{bmatrix}, \quad (5.33)$$

Decomposing (5.33) as below

$$E\{X[i]X^H[j]\} = \mathbf{E}_i^H \overline{\mathbf{R}}\, \mathbf{E}_j\,, \qquad i = 0,1,\dots,(k_B-1), \qquad j = 0,1,\dots,(k_B-1), \tag{5.34}$$

Where $\mathbf{E}_k$, $k = 0,\dots,(k_B-1)$ and $\overline{\mathbf{R}}$ can be defined as in (5.35) and (5.36), respectively.

$$\mathbf{E}_k \triangleq \begin{bmatrix} e_k & 0 & \dots & 0 \\ 0 & e_k & \dots & 0 \\ \vdots & 0 & \ddots & \\ \vdots & \vdots & \vdots & \vdots \\ 0 & 0 & \dots & e_k \end{bmatrix}, \tag{5.35}$$

$$\overline{\mathbf{R}} \triangleq \begin{bmatrix} \mathbf{R}_{1,1} & \mathbf{R}_{1,2} & \dots & \mathbf{R}_{1,M} \\ \mathbf{R}_{2,1} & \mathbf{R}_{2,2} & \dots & \mathbf{R}_{2,m} \\ \vdots & \vdots & \ddots & \vdots \\ \mathbf{R}_{M,1} & \mathbf{R}_{M,2} & \dots & \mathbf{R}_{M,M} \end{bmatrix}. \tag{5.36}$$

Where, $\mathbf{R}_{m,n}$, $m = 1,\dots,M$ and $n = 1,\dots,M$ represents the cross-correlation between m^{th} and n^{th} data received from sensors array (Note that m^{th} data is collected by the sensor number m). Using (5.33) in (5.29) would result in the correlation matrix $\mathbf{R}_|$ as follow:

$$\mathbf{R}_| = \begin{bmatrix} \mathbf{E}_0^H \overline{\mathbf{R}}\, \mathbf{E}_0 & \mathbf{E}_0^H \overline{\mathbf{R}}\, \mathbf{E}_1 & \dots & \mathbf{E}_0^H \overline{\mathbf{R}}\, \mathbf{E}_{(k_B-1)} \\ \mathbf{E}_1^H \overline{\mathbf{R}}\, \mathbf{E}_0 & \mathbf{E}_1^H \overline{\mathbf{R}}\, \mathbf{E}_1 & \dots & \mathbf{E}_1^H \overline{\mathbf{R}}\, \mathbf{E}_{(k_B-1)} \\ \vdots & \vdots & & \vdots \\ \mathbf{E}_{(k_B-1)}^H \overline{\mathbf{R}}\, \mathbf{E}_0 & \mathbf{E}_{(k_B-1)}^H \overline{\mathbf{R}}\, \mathbf{E}_1 & \dots & \mathbf{E}_{(k_B-1)}^H \overline{\mathbf{R}}\, \mathbf{E}_{(k_B-1)} \end{bmatrix}. \tag{5.37}$$

Since the matrix $\mathbf{E}$ can be written as:

$$\mathbf{E} = \left[\mathbf{E}_0\ \mathbf{E}_1\ \dots \mathbf{E}_{(k_B-1)}\right], \tag{5.38}$$

it can be considered as a block DFT operator and $\mathbf{R}_|$ can be re-write as:

$$\mathbf{R}_| = \mathbf{E}^H \overline{\mathbf{R}}\, \mathbf{E}. \tag{5.39}$$

Inserting (5.39) into (5.27) will result in output power of the DFT-based BF under BP mode as it shown below:

$$P = \frac{1}{(k_B)^2}\, \boldsymbol{w}^H F_n \mathbf{E}^H \overline{\mathbf{R}}\, \mathbf{E}\, F_n^H \boldsymbol{w}, \qquad n = 0,1, \dots, (k_B - 1). \tag{5.40}$$

Using (2.11) for uncorrelated baseband signals in (5.35) will give:

$$\mathbf{R}_{m.n} = E\{\tilde{x}_m \tilde{x}_n^H\}$$

$$= \exp\{j2\pi f_c(\tau_{1,m_1} - \tau_{1,m_2})\}$$

$$\times \begin{bmatrix} r_1(\tau_{1,m_1} - \tau_{1,m_2}) & r_1(-T_s + \tau_{1,m_1} - \tau_{1,m_2}) & \dots & r_1(-(k_B - 1) + \tau_{1,m_1} - \tau_{1,m_2}) \\ r_1(T_s + \tau_{1,m_1} - \tau_{1,m_2}) & r_1(\tau_{1,m_1} - \tau_{1,m_2}) & & r_1(-(k_B - 2) + \tau_{1,m_1} - \tau_{1,m_2}) \\ \vdots & \vdots & \ddots & \vdots \\ r_1((k_B - 1) + \tau_{1,m_1} - \tau_{1,m_2}) & r_1((k_B - 2) + \tau_{1,m_1} - \tau_{1,m_2}) & \dots & r_1(\tau_{1,m_1} - \tau_{1,m_2}) \end{bmatrix} +$$

$$\exp\{j2\pi f_c(\tau_{2,m_1} - \tau_{2,m_2})\}$$

$$\times \begin{bmatrix} r_2(\tau_{2,m_1} - \tau_{2,m_2}) & r_2(-T_s + \tau_{2,m_1} - \tau_{2,m_2}) & \dots & r_2(-(k_B - 1) + \tau_{2,m_1} - \tau_{2,m_2}) \\ r_2(T_s + \tau_{2,m_1} - \tau_{2,m_2}) & r_2(\tau_{2,m_1} - \tau_{2,m_2}) & & r_2(-(k_B - 2) + \tau_{2,m_1} - \tau_{2,m_2}) \\ \vdots & \vdots & \ddots & \vdots \\ r_2((k_B - 1) + \tau_{2,m_1} - \tau_{2,m_2}) & r_2((k_B - 2) + \tau_{2,m_1} - \tau_{2,m_2}) & \dots & r_2(\tau_{2,m_1} - \tau_{2,m_2}) \end{bmatrix} +$$

$$\exp\{j2\pi f_c(\tau_{D,m_1} - \tau_{D,m_2})\}$$

$$\times \begin{bmatrix} r_D(\tau_{D,m_1} - \tau_{D,m_2}) & r_D(-T_s + \tau_{D,m_1} - \tau_{D,m_2}) & \dots & r_D(-(k_B - 1) + \tau_{D,m_1} - \tau_{D,m_2}) \\ r_D(T_s + \tau_{D,m_1} - \tau_{D,m_2}) & r_D(\tau_{D,m_1} - \tau_{D,m_2}) & & r_D(-(k_B - 2) + \tau_{D,m_1} - \tau_{D,m_2}) \\ \vdots & \vdots & \ddots & \vdots \\ r_D((k_B - 1) + \tau_{D,m_1} - \tau_{D,m_2}) & r_D((k_B - 2) + \tau_{D,m_1} - \tau_{D,m_2}) & \dots & r_D(\tau_{D,m_1} - \tau_{D,m_2}) \end{bmatrix} +$$

$$\begin{bmatrix} r_w(0) & 0 & \dots & 0 \\ 0 & r_w(0) & \dots & 0 \\ \vdots & \vdots & \ddots & \vdots \\ 0 & 0 & \dots & r_w(0) \end{bmatrix}, \qquad m_1 = 1,2, \dots, M \text{ and } m_2 = 1,2, \dots, M \tag{5.41}$$

Expected value function is a linear function, therefore, arrays of $\overline{\mathbf{R}}$ in (5.35) could be denoted as:

$$\mathbf{R}_{m,n} = \mathbf{R}_{(m,n),s_1} + \mathbf{R}_{(m,n),s_2} + \dots + \mathbf{R}_{(m,n),s_D}\,,$$
$$m = 1,2, \dots, M \text{ and } n = 1,2, \dots, M \tag{5.42}$$

Here, $\mathbf{R}_{(m,n),s_d}, m = 1,2, \dots, M,\ n = 1,,2 \dots, M$ and $d = 1,2, \dots, D$ represents the cross-correlation matrix between the observation of the signal source S_d which is

collected by the m^{th} and n^{th} element of the ULA. Thus (5.35) can be extend for overall observations as bellow:

$$\bar{\mathbf{R}} = \bar{\mathbf{R}}_{s_1} + \bar{\mathbf{R}}_{s_2} + \ \ldots + \bar{\mathbf{R}}_{s_D} . \tag{5.43}$$

Consequently, inserting (5.43) into (5.40) would result in the contribution of each output signal's power from the overall output power of the DFT-based BF using BP mode as:

$$P[n] = \frac{1}{(k_B)^2}\, \boldsymbol{w}^H F_n \mathbf{E}^H \left(\bar{\mathbf{R}}_{s_1} + \bar{\mathbf{R}}_{s_2} + \ \ldots + \bar{\mathbf{R}}_{s_D}\right) \mathbf{E}\, F_n^H \boldsymbol{w},$$
$$P[n] = P_{s_1}[n] + \cdots + P_{s_D}[n] + P_w[n], \qquad n = 0, \ldots, (k_B - 1). \tag{5.44}$$

Finally, the SINR of the DFT-based BF under BP mode scenario could be calculated as:

$$SINR_{DFT-BP} = \frac{P_{s_1}[n]}{P_{s_2}[n] + \cdots + P_{s_D}[n] + P_{\mathrm{w}}[n]}, \qquad n = 0, \ldots, (N-1) \tag{5.45}$$

where the out power of the d^{th} source can be obtained from

$$P_{s_d}[n] = \frac{1}{(k_B)^2}\, \boldsymbol{w}^H F_n \mathbf{E}^H \bar{\mathbf{R}}_{s_d} \mathbf{E}\, F_n^H \boldsymbol{w}, \qquad d = 1, 2, \ldots, D \tag{5.46}$$

And $P_{\mathrm{w}}[n]$ is the output power of the noise as follow

$$P_{\mathrm{w}}[n] = \frac{1}{(k_B)^2}\, \boldsymbol{w}^H F_n \mathbf{E}^H \bar{\mathbf{R}}_{\mathrm{w}} \mathbf{E}\, F_n^H \boldsymbol{w} = \frac{r_{\mathrm{w}}(0)}{(k_B)^2} \parallel \mathbf{E}\, F_n^H \boldsymbol{w} \parallel^2, \quad n = 0, \ldots, (N-1), \tag{5.47}$$

Computation of the DFT-based BF's output SINR can be summarized as in 4 steps below:

Step(1): Construct the matrix $\mathbf{E}$ using (5.35) and (5.38) and the definition of e_k as in (5.27).

Step(2): Calculate the matrix F_n from (5.26) for $n = 0, \ldots, (N-1)$.

Step(3): Calculate the power of signals and noise for the DFT-based BF from (5.46) and (5.47). Consequently, calculate the output SINRs according to (5.45).

Step(4): Afterward, set n to $(n+1)$ and go back to second step. Pending $n \geq (k_B - 1)$, select $SINR[n]$ instead of $SINR[n - k_B]$.

5.6 Signal to Interference Plus Noise Ratio Formulation for the DFT-Based Beamformer Under Sliding Window Mode

In SW processing, each cycle of the BF only generates a new output, which it is the first element of the BF output $y[0]$ in purposed cycle. Since, for $n = 0$ in, the matrix F_n would reduce to identity matrix with size Mk_S, the power at the output of the DFT-based BF under SW processing (DFT-SW) can be write as:

$$P_{\text{DFT-SW}}[0] = \frac{1}{{k_s}^2}\, \boldsymbol{w}^H \mathbf{E}^H \bar{\mathbf{R}}\, \mathbf{E}\, \boldsymbol{w}, \tag{5.46}$$

$$P[0] = P_{s_1}[0] + P_{s_2}[0] + \ \ldots + P_{s_D}[0] + P_{\text{w}}[0].$$

And the SINR of the SW processing can be computed using each time instant $(t = 0)$ in each cycle of the DFT-SW, on which in each cycle, one new sample is just generated. Thus SINR of the DFT-SW is given by:

$$SINR_{DFT-SW}[0] = \frac{P_{s1}[0]}{P_{s_2}[0] + \ \ldots\ldots + P_{s_D}[0] + P_{\text{w}}[0]}, \quad \text{for each slide.} \tag{5.47}$$

Here, calculation of the output SINR of the DFT-based BF using SW processing can be summarized in 3 steps below:

Step(1): Construct the matrix **E** using (5.35) and (5.38) and the definition of e_k as in (5.27). Note that matrix F_n has reduced to identity matrix.

Step(2): Calculate the power of the signals and noise for the DFT-based BF from (5.46) and (5.47). Consequently, compute the output SINRs according to (5.45).

Step(3): For all time instants n, set $SINR[n] = SINR[0]$.

Chapter 6

PERFORMANCE ANALYSIS of DFT-BF

In the literature, broadband beamforming has been broadly considered. Wideband BFs are generally designed to obtain high spatial resolution and have applications in various fields such as communications, acoustics, bio-medics and military. In comparison to their narrowband counterparts wideband BFs require considerably large spatial and temporal dimensions. To achieve high resolution large number of TDL elements (L) and sensors (M) are required. However, this increase in L and M would lead to a very high computational complexity for wideband beamforming techniques. To decrease the computational complexity of the broadband BFs a transformation such as DFT can be used to deal with different frequencies separately as in the case of a narrowband BF.

The rest of this chapter provides information about the simulation setup and investigates the performance of a DFT-based BF under block processing (BP) and sliding window (SW) modes when correlation matrices are either known or estimated for a finite number of samples. The SINR criterion is used to assess the performance of the DFT-based BF. Afterward, the Ensemble Mean Squared Error (EMSE) is utilized to show the error between the input SINR and the output SINR. At the end, the computational complexity for BP and SW modes was compared in terms of Multiply-ACcumulates (MACs) operations.

6.1 Simulation Parameters

Simulations were carried out using the MATLAB platform assuming an 8 element ULA ($M = 8$) with inter element spacing of $\lambda/2$ and three baseband incoming signals each with bandwidths $B = 50MHz$, central frequencies of $150MHz$ and DOAs of $\theta_1 = 20^{\circ}$, $\theta_2 = 40^{\circ}$ and $\theta_3 = -20^{\circ}$. The signal with direction $\theta_1 = 20^{\circ}$was assumed to be the desired signal and individual powers for the three different sources were respectively set at $P_{s_d} = 5, 10, 10\ (dB)$ over the noise level. Each sensor's output was sampled at Nyquist rate of $1/2B$. All sources plus the noise were simulated using zero mean mutually uncorrelated white random Gaussian processes. For a fair comparison between the DFT-based BF under BP and SW processing modes, length of the signals were set at $N = 1000$ and total number of samples was fixed at 8000 ($M \times N$).

6.2 Power Spectral Density and Autocorrelation

The power spectral density, $S_x(f)$, of a wideband signal $x[n]$ with constant power level P_x inside the band $[-B, B]$ and zero outside can be expressed as:

$$S_x(f) = \begin{cases} P_x, & -B \leq x \leq B \\ 0, & else \end{cases} . \tag{6.1}$$

The corresponding correlation sequence of the signal $x[n]$ will then be:

$$r_x[n] = 2BP_x sinc(2Bn) . \tag{6.2}$$

Since output of each sensor in the sensor array is sampled at Nyquist rate, this guarantees that each sample is uncorrelated with the others. Hence, the correlation sequence can be written as:

$$r_x[n] = \begin{cases} 2BP_x, & x = 0 \\ 0, & x \neq 0 \end{cases} . \tag{6.3}$$

Figure 6.1 below depicts the power spectral density (PSD) and the corresponding

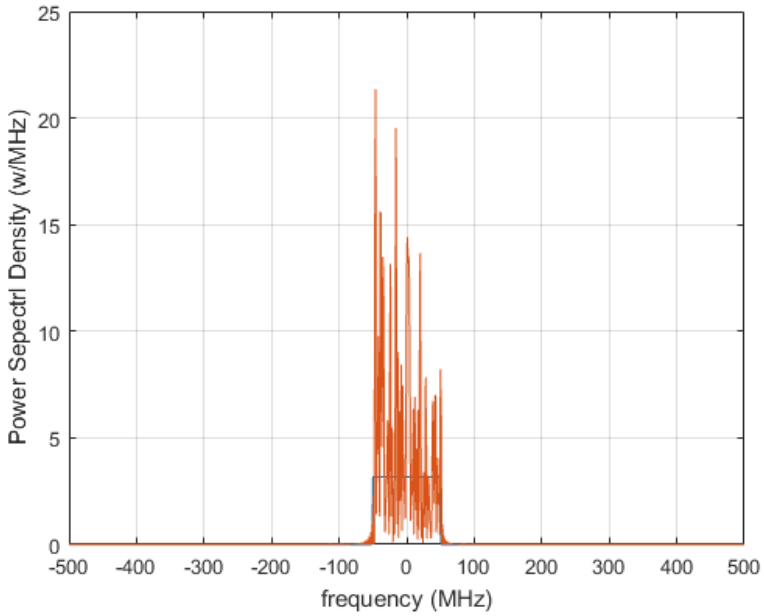

(a)

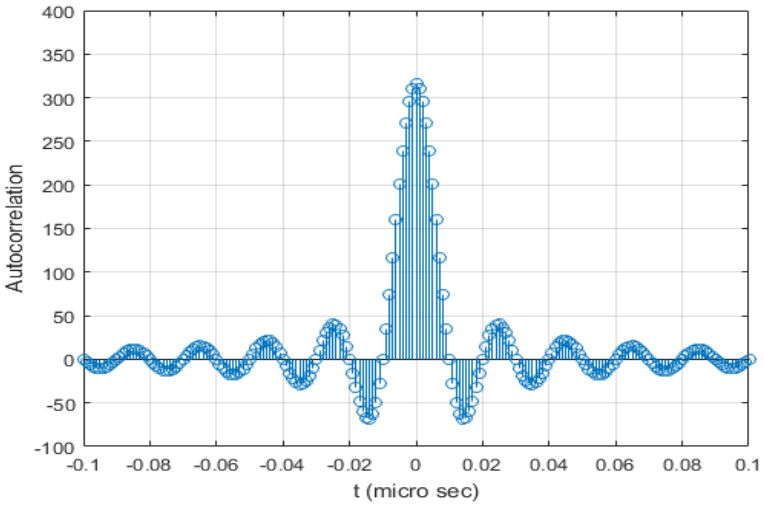

(b)

Figure 6.1: Power Spectral Density and Autocorrelation for a White Gaussian Random Process (WGRP) for Bandwidth of 50 MHz:
(a) PSD of the proposed band-limited WGRP,
(b) Correlation function of the band-limited WGRP.

autocorrelation function of a wideband signal with 5 dBW/MHz power level above noise level. The approximation method reported in [20] has been used to generate the waveform for a band-limited white Gaussian random process assuming a fixed power level. Afterwards this signal has been sampled at Nyquist rate. The realization of this sampled signal is as depicted in Fig. 6.2. Also note that Fig. 6.1(a) has the periodogram approximation of this signal (the solid brown line).

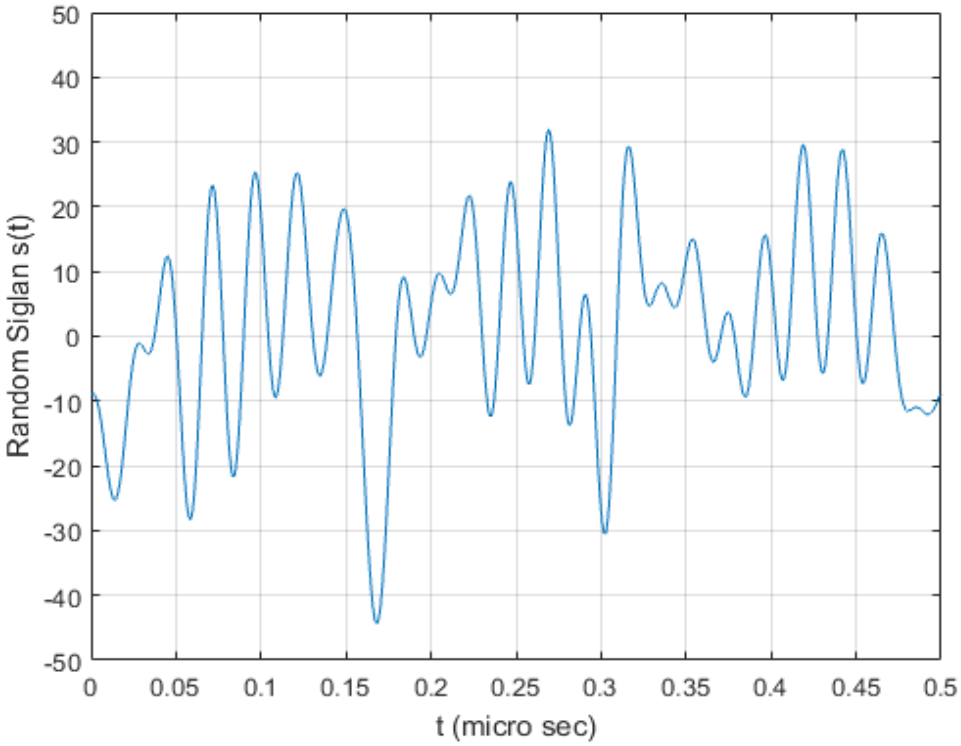

Figure 6.2: An Observation of a Band-Limited WGRP.

Output SINRs for DFT-based BF have been computed generating weight vectors with or without finite sample effect. For the ideal scenario without finite sample effect the autocorrelation matrices required for producing the weight vectors were assumed known and the output SINRs for DFT-based BF under BP mode has been obtained using 25, 50, 100, 200 and 1000 blocks (respective block sizes of $40, 20, 10, 5$ and 1) and are as depicted in Fig. 6.3(a). Figure 6.3 (b) depicts the output SINRs of the DFT-based BF under BP mode without knowing the correlation matrices (need to estimate $\widehat{\mathbf{R}}_k$s). Spatial smoothing as in (5.11) has been used to estimate the correlation functions for same number of block as in Fig. 6.3(a). The impact of the number of frequency bins (k_B) without and with finite sample effect has been demonstrated in Fig 6.3(a) and (b). observing the plots, we note that the

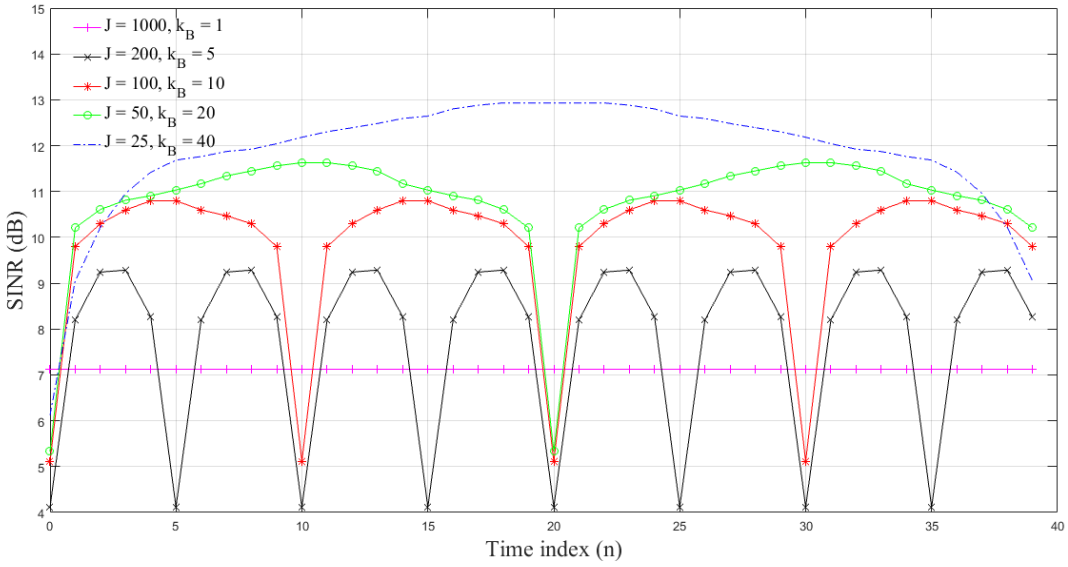

(a)

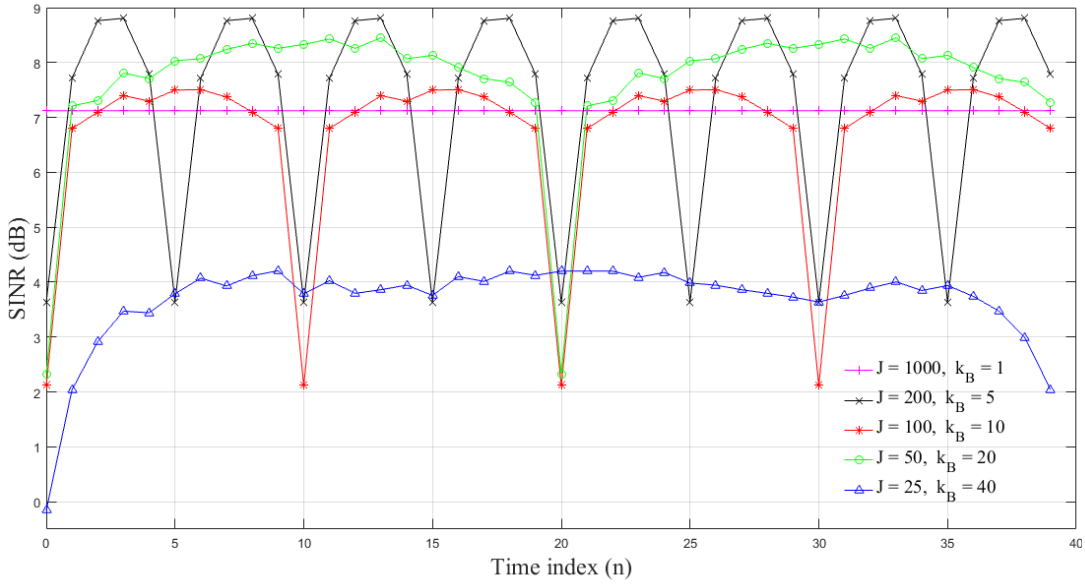

(b)

Figure 6.3: Performance of DFT-Beamformer Under Block Processing With and Without Finite Sample Effect for $N = 1000$ snapshots:
(a) Corresponding SINRs for DFT-beamformer under BP with different number of blocks and with known correlation matrices,
(b) The SINRs at the output of the DFT-based beamformer under block processing mode with different block's sizes and with estimated correlation matrices using (5.11).

output SINR of the DFT-based BF is time varying regardless of the finite sample effect. In fact, the SINRs curves are periodic and their period equals the number of frequency bins used. Due to the hill shape of the SINR curves, it could be understood

that the best SINR would be achieved at time index $n = \lfloor k_B/2 \rfloor$ for both with and without finite sample effect. For the case of no finite sample effect (Fig. 6.3(b)) it can be seen that by increasing the number of frequency bins (k_B) the BF improves the peak SINR. However, for the fixed number of data snapshots (N), there would be a compromise between number of snapshots in a block (k_B), and the number of blocks (J) which could be seen from Fig. 6.3 (b).

When the DFT-based BF operating under BP mode has higher number of frequency bins (accordingly smaller block size) the estimate of the correlation matrices $\left(\widehat{\mathbf{R}}_k, k = 1, \dots, k_B\right)$ would be poorer and the SINR performance will degrade. As can be seen from the Fig. 6.3 (b), selecting $J = 200$ and $k_B = 5$ will result in highest peak among all different settings, but the SINR value for $J = 200$ could be smaller in comparison with the narrowband MVDR case $(J = 1000,\ k_B = 1)$ at the time instant $n = 0$. For SINR plots with finite sample effect, generally the overall output SINR is weakened when k_B is increased from 5 to 40. For $J = 25$ and $k_B = 40$ the SINR under DFT-based BF would become worse (lower) than the SINR for the narrowband MVDR case. Fig. 6.4 shows that the Ensemble-Mean-Squared-Error (EMSE) for both scenarios (with and without finite sample effect). EMSE will increase when less number of blocks is used (larger block size). In other words, selecting larger block sizes (k_B) when number of snapshots is fixed would result in a lower SINR. However, as depicted in Fig. 6.6 when higher number of blocks is used then the computational complexity would rise. The DFT-based BF using SW mode will give just one sample in each cycle. Therefore, the output SINR for each cycle could be calculated at time instant zero. The output SINRs for DFT-based BF using SW mode for various window

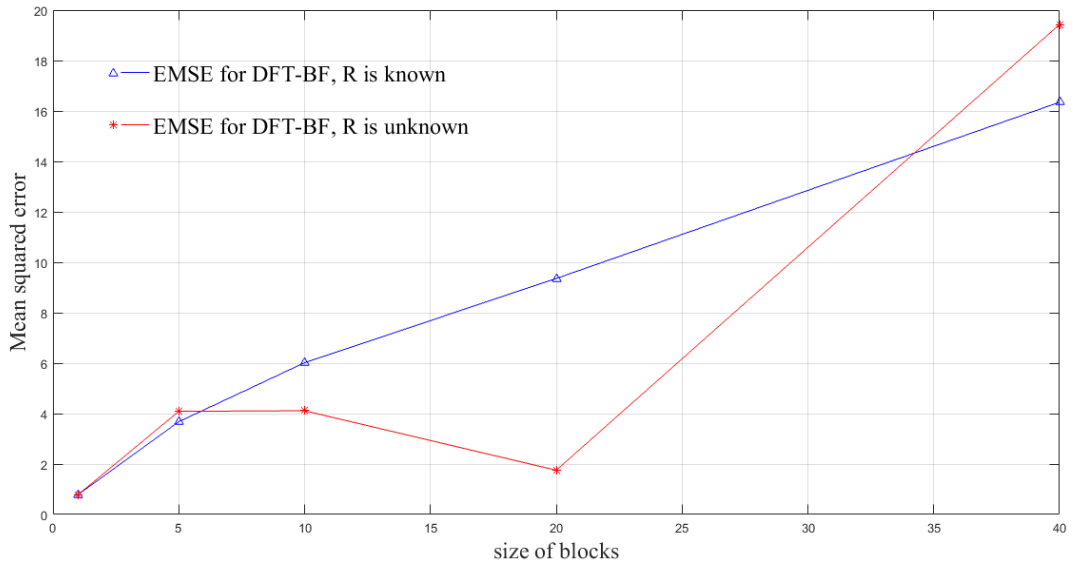

Figure 6.4: Ensemble-Mean-Squared-Error (EMSE) Between the Input and Output SINRs of the DFT-BF Using BP Given Different Block Sizes.

sizes have been plotted in Fig. 6.5. Note that as the window size selected becomes larger the SINR at the output of the DFT-based BF under SW mode will become lower.

In this thesis the computational complexities for BP and SW modes were also calculated and compared in terms of Multiply-ACcumulates (MACs) operations. As stated in [21], for M sensors and L-TDL elements the cost of the DFT-based BF under BP mode can be calculated as:

$$C_{DFT-BP} = (M+1)\log_2 L + M^2 + 3M. \tag{6.4}$$

This is a cost per full-band sampling period. The cost for SW mode in MACs is slightly higher since under the SW mode the DFT is computed at each time instant n and IDFT is replaced by a summation as stated in [9]. The MAC cost for SW can be calculated using:

$$C_{DFT-SW} = L(M\log_2 L + M^2 + 3M)\,. \tag{6.5}$$

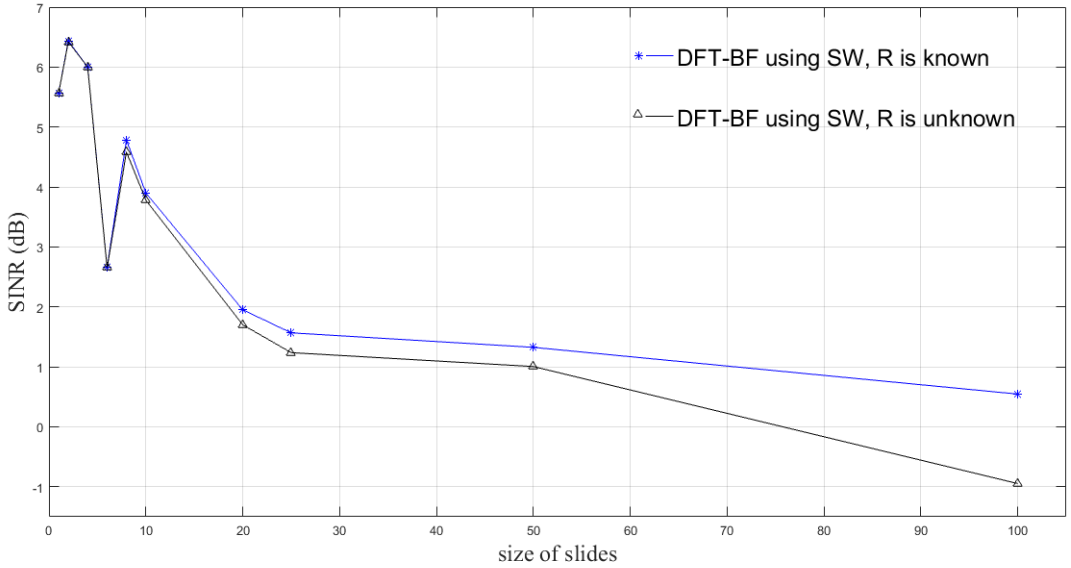

Figure 6.5: Output SINR for DFT-based Beamformer Using SW Processing [Window sizes of $k_s = 1, 2, 4, 6, 8, 10, 20, 25, 50$ and 100 at time instant $n = 0$].

Figure 6.6. depicts the cost in MACs for DFT-based BF under both BP and SW mod-

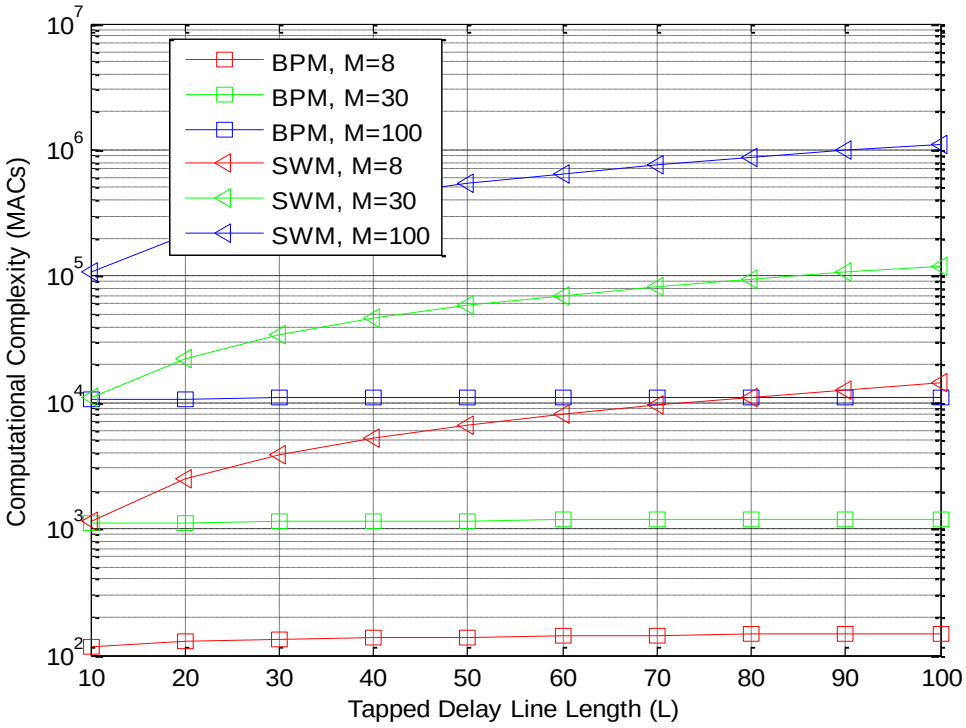

Figure 6.6: Computational Complexities in MACs
(Block Processing Mode is denoted by BPM and the
Sliding Window Mode is denoted by SWM)

-es for various number of TDL elements (L), and $M = 10, 30$ and 100 sensors (Note that the TDLs length is equal to the block or window sizes ($L = k_B \; or \; k_S$)). Clearly for the DFT-based BF the cost under BP mode is much lower in comparison to the cost under SW processing.

6.3 Real Life Based Analysis

While the voice services in 3G were using circuit-switching, todays 4G LTE networks use packet switching. These packet switched services can integrate with other services and applications such as messaging, video calling, Web applications, and other mobile applications. WebRTC is an open project supported by Google, Mozilla, and Opera within the Internet Engineering Taskforce (IETF) that enables real-time communications in Web browsers via JavaScript APIs. 3GPP Release 12 specifications define how WebRTC clients can access IMS services, including packet voice and video communication.

WebRTC is able to access device hardware, such as microphones or cameras, without the need to install a plugin or preload a dedicated communication application, such as Skype or Viber. Also when compared to VoLTE has the advantage that it is platform and device independent and is also open for development by third party developers.

Because WebRTC is built into the browser, a lot of apps that incorporate voice and video as elements of a larger communications application will use it. It is expected that WebRTC along with voice over LTE (VoLTE) become the two leading real-time communication tools for future generations of mobile communications.

This section of the thesis provides the SINR performance of a DFT-BF under BP mode

when WebRTC with 50 participants is assumed for video conferencing in Advance Long Term Evaluation (A-LTE) network. The uplink and downlink frequencies for A-LTE (F_{downling} and F_{uplink}) can be calculated using (6.6):

$$F_{\text{downlink}} = F_{\text{DL\_Low}} + 0.1\,(N_{\text{DL}} - N_{\text{DL\_offset}})$$
$$F_{\text{uplink}} = F_{\text{UL\_Low}} + 0.1\,(N_{\text{UL}} - N_{\text{UL\_offset}}) \quad (6.6)$$

Where, N_{DL} is downlink E-UTRA Absolute Radio Frequency Channel Number (EARFCN), N_{UL} is uplink EARFCN, $N_{\text{DL\_offset}}$ is the offset used to calculate downlink EARFCN and $N_{\text{UL\_offset}}$ is the offset used to calculate uplink EARFCN using Table 6.1:

Table 6.1: EARFCN to frequency conversion for downlink and uplink

E-UTRA band	**F_{DL_Low} (MHz)**	**N_{DL_Offset}**	**downlink EARFCN (N_{DL})**	**F_{UL_Low} (MHz)**	**N_{UL_Offset}**	**uplink EARFCN (N_{UL})**
1	2110	0	0-599	1920	18000	18000-18599
2	1930	600	600-1199	1850	18600	18600-19199
3	1805	1200	1200-1949	1710	19200	19200-19949
4	2110	1950	1950-2399	1710	19950	19950-20399

In this last simulation we have assumed an 8 element ULA ($M = 8$) with inter element spacing of $\lambda/2$ and three baseband incoming signals each in the third E-UTRA band of A-LTE channel with bandwidths of $B = 3.5\,MHz$, central frequencies of $1.7475\,MHz$ and DOAs of $\theta_1 = 20^{\circ}$, $\theta_2 = 40^{\circ}$ and $\theta_3 = -20^{\circ}$. The signal with

direction $\theta_1 = 20^{\circ}$ was assumed to be the desired signal and individual powers for the three different sources were respectively set at $P_{s_d} = 10, 5, 30$ (dB) over the noise level. Each sensor's output was sampled at Nyquist rate of $1/2B$. All sources plus the noise were simulated using zero mean mutually uncorrelated white random Gaussian processes. Length of the signals were assumed to be $N = 1000$ and with 8 sensors total number of samples ($M \times N$) is 8000.

Output SINRs for DFT-based BF have been computed generating weight vectors with finite sample effect. Figure 6.7 depicts the output SINRs of the DFT-based BF under BP mode without knowing the correlation matrices (need to estimate $\widehat{\mathbf{R}}_k$s). Spatial smoothing as in (5.11) was used to estimate the correlation functions. From Fig 6.7 we observe that when the DFT-based BF operating under BP mode uses higher number of frequency bins (accordingly smaller block size) the estimate of the correlation matrices $\left(\widehat{\mathbf{R}}_k\ , k = 1, \dots, k_B\right)$ and the SINR performance would be poorer. Selecting $J = 25$ and $k_B = 40$ will result in highest peak among all different settings, however $J = 100$ and $k_B = 10$ only has new deeps in the SINR plot and perhaps is the best setting.

For $J = 200$ and $k_B = 5$ the SINR under DFT-based BF would become lower than sthe SINR for the narrowband MVDR case ($J = 1000$ and $k_B = 1$).

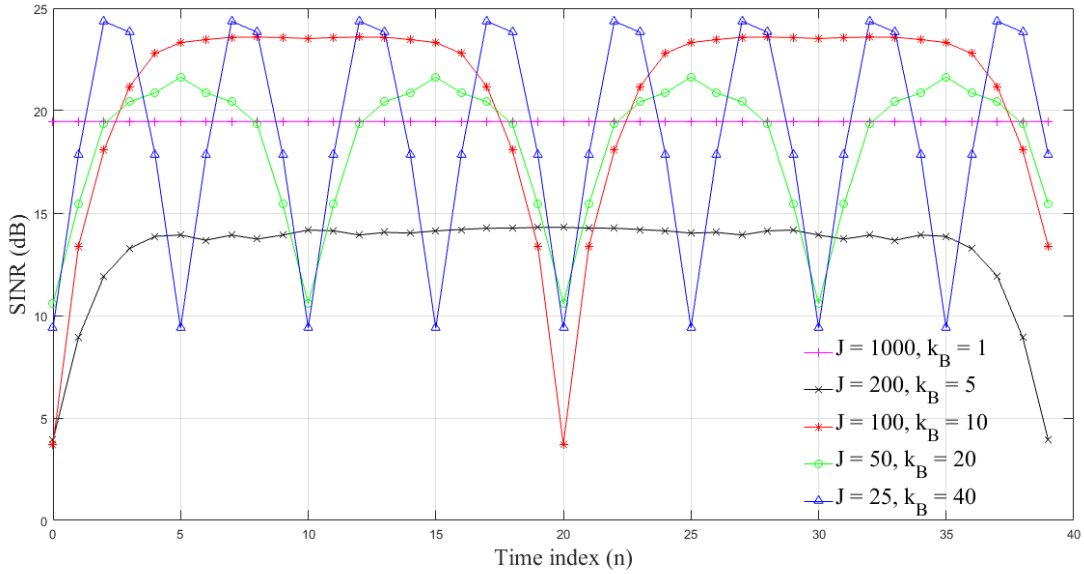

Figure 6.7: Performance of DFT-BF Under 4G A-LTE Network Assuming Finite Sample Effect.

Chapter 7

CONCLUSION AND FUTURE WORKS

7.1 Conclusion

The SINRs at the output of the DFT-based BFs under real correlation matrices and estimated correlations under finite sample effect, are examined in this thesis. According to this study, it is figured out that the DFT-based BFs have high proficiency to solve the wideband sources problem. However, the number of bins k_B or k_S have to be carefully selected especially when the overall samples are finite. On the other hand, the number of blocks/slides are very important factor in changing the computational complexities and the accuracy of the correlation matrices. Although, the higher number of blocks are resulted in better correlation estimations but, separating the bandwidth of received signal to more frequency bins doesn't necessarily result in better performance under the limited sample environment. On the other hand, taking higher number of blocks will result in logarithmic increase on the computational complexities. Additionally, the output SINR of the DFT-based BF using BP mode at different time instants n would be varying. Due to our simulations, the DFT-based BF under BP scenario would perform well results in the middle time instant at each block $(n = \lfloor k_B/2 \rfloor)$ and the worst ones would be occur at the starting $(n = 0)$ and ending $(n = k_B - 1)$ frequency bins of the blocks. Also the impact of the finite sample effect on DFT-based wideband BFs can be solved using BP investigation. Therefore, it isn't necessary to concern about finite sample effect.

Since the DFT-based BF utilizing SW process always takes a new snapshot and generate only one sample at its output (at $n = 0$) and suffers from the highly correlated inputs and it gives acceptable results just for small number of slides, these findings shows that the DFT-based BF using SW needs to replace by a new structure with the enhanced performance in comparison with the existing approach. In addition to these shortcomings of the DFT-based BF using SW process the computational complexities of this method is considerably higher than the DFT-based BF using BP procedure.

7.2 Future Work

Both the BP and SW modes of the DFT-based BF will neglect any correlation that may exist between the frequency bins. However as suggested by [22] overlap-add or overlap-save approaches can be applied to deal with the problem of internal correlations between frequency bins. Also, since DFT-based BF under BP scenario has worse performance at the start and end points of each block it would be useful to utilize a padding technique between the blocks.

REFERENCES

[1] Johnson, D. H. and Dudgeon, D. E. (1993). *Array Signal Processing: Concept and techniques*, (1st ed.). Prentice Hall, Engeglewood Cliffs, New Jersy.

[2] Kennedy, R. A., Abhayapala T. D. and Ward, D. B., (1998, August 6). Broadband Nearfield Beamforming Using a Radial Beampattern Trasformation. *IEEE Transaction on Signal Processing, 46(8*), 2147-2156. doi:10.1109/78.705426

[3] Van Veen, B .D. and Buckley, K. M. (1988, April). Beamforming: A versatile approach to spatial filtering. *Acoustic on Signal Processing Magezine, 5,* (pp. 4-24).

[4] S Weiss, S. and Stewart, R.W. (2000, August). Fast implementation of over sampled modulated filter banks. *Electroninc Letter, 36,* (pp. 1502-1503).

[5] Weiss, S. (2000). Analysis and fast implementation of oversampled filter banks. in *International Conferance on Mathematics in Signal Processing,* Warwick.

[6] Moon, S. H., Han, D. S., Cho, M. J. and Par, K. H. (1999, October). Frequncey domain GSC with low computational complexsity. in *IEEE Military Communication Conferance Proceedings,* Atlantic.

[7] Leng, K. C. (2009, October). Broadband Adaptive Beamforming with Low Coplexity and Frequency Invariant Response. Univercity of Southhampton, Southampton.

[8] Justice, J. H., Owley, N. L., Yen, J. L. and Kak, A. C. (1984). *Array Signal Processing*, (1st ed.). in S. Haykin, (Ed), Prentice Hall, Englewood Cliffs, New Jersey.

[9] Trees, H. L. V. (2002). *Optimum Array Processing*, (4th ed.), (p. 1472), John Wiley &Sons, Inc., New York.

[10] Phillai, S. U. (1989). *Array Signal Processing*, Springer-Verlag, New York.

[11] Krim, H. and Viberg, M. (1996, July). Two decades of array signal processing research: the parametric approach. *IEEE Signal Process. Mag., 13 (4)*, (pp. 67-94), IEEE, USA.

[12] Krim, H. and Viberg, M. (1995). Sensor Array Signal Processing: Two Decades Later. Stochastic Sys. Group, Massachussets Institute of Technology Cambridg Univercity.

[13] Wen, L. Y. (2012, April) Fourier Trasform Applications. in *Hilbert Transform and Applications*, D. Salih, (Ed.), (pp. 291- 300), Shanghai, Chaina, In Tech.

[14] Williams, A. and Taylor, F. J. (2006, July 31). *Electronic Filter Design Handbook,* (4th ed.), McGraw-Hill Education, Columbus, USA.

[15] Oppenheim, A. V. and Schefer, R. W. (2009, Agust 28). *Disceret-Time Signal Processing,* (3rd ed.), T. Robins, (Ed.), Pearson, New Jersey.

[16] Zatman, M. (1998). How narrow is narrowband? *IEEE proceeding, 145(1),* (pp. 85-91), IEEE, USA.

[17] Abhayapala, P. (1999). Modal Analysis and Synthesis of Broadband Nearfield Beamforming. *Australian National University,* Australia.

[18] Kopp, L. and Bienvenu, G. (1985, My). Methodes Haute Resolution Apres Formation de Voies. in *International Conference du GRETSI*, Nice, France.

[19] Godara, L. C. (1995, July). Application of the fast Fourier transform to broadband beamforming. *Journal of Acoustic Society American, 98(1),* (pp. 230-240).

[20] Miller, S. L. and Childers, D. (2004). Simulation Techniques. in *Probability and Random Processes with Applications to Signal Processing and Communications*, (pp. 457-480), Boston, Elsevier.

[21] S., Weiss, C.L. Koh and W. Liu, (2005). A comparison of adaptive beamforming implementations for wideband scenarios, in *IEE/EURASIP International Conference*, (pp. 28/1-28/7).

[22] Weiss, S., Stenger, A., Stewart, R. W. and Rabenstein, R. (2002, Agust 7). Stady-State Performance Limitations of Subband Adaptive Filters. *IEEE Transaction on Signal Processing, 49(9),* (pp. 1982-1991).

[23] Weiss, S. and Proudler, I. K. (2002). Comparing Efficient Broadband Beamforming Architectures and Their Performance Trade-Offs. *14th International conference on Proceedings DSP,* Santorini, Greece.

[24] Kellerman, W. and Buchner, H. (2003). Wideband Algirithms Versus Narrowband Algorithms for Adaptive Filtering in the DFT Domain. in *Asilomar Conference on Signal and Systems Computers,* Nuremberg, Germany.

[25] Crochiere, R. E. and Rabiner, L. R. (1983, March 21). *Multirate Digital Signal Processing,* (1st ed.), Pearson, p. 411.

[26] Shynk, J. J. (1992). Frequency-Domain And Multirate Adaptive Filternig. *IEEE Signal Processing Magazine, 9(1),* (pp. 14-37).

[27] Trees, H. L. V. (2005). *Optimum Array Processing*. (4th ed.), Wiley-Interscience, p. 1472.

[28] Proakis, J.G. and Manolakis, D. G. (1996). *Digital Signal Processing: Principles Algorithms and Aplications*. (4th ed.), Prentice Hall.

[29] Koh, C. L. (2009, October). Broadband Adaptive Beamforming with Low Coplexity and Frequency Invariant Response, *Univercity of Southhampton*, Southampton.

[30] Liu, Y. W. (2012, April). Fourier Trasform Applications, in *Hilbert Transform and Applications*, D. S. Salih, Ed., Shanghai, Chaina, In Tech, (pp. 291- 300).

[31] Manolakis , D. G. and Proakis, J. G. (1996) *Digital Signal Processing: Principles Algorithms and Aplications,* Prentice Hall, (4th ed.), London, UK.

[32] Gold Stein, J. S. and Reed, L. S. (1997). Theory of partially adaptive radar, *IEEE transaction on Aerospace and electronic system, 33(2),* (pp. 1309-1325).

[33] Benesty, J., Chen, J. and Huang, Y. (2008). *Microphon array signal processing*, Berlin: Springer-verlag Berlin Heidelberg.

[34] Reen, K. (2008). *A Study of The Gibbs Phenomenon in Fourier Series and Wavelets*, Ms Thesis, Mexico City.